Contract No:

This document was prepared in conjunction with work accomplished under Contract No. 89303321CEM000080 with the U.S. Department of Energy (DOE) Office of Environmental Management (EM).

Disclaimer:

This work was prepared under an agreement with and funded by the U.S. Government. Neither the U.S. Government or its employees, nor any of its contractors, subcontractors or their employees, makes any express or implied:

1) warranty or assumes any legal liability for the accuracy, completeness, or for the use or results of such use of any information, product, or process disclosed; or
2) representation that such use or results of such use would not infringe privately owned rights; or
3) endorsement or recommendation of any specifically identified commercial product, process, or service.

Any views and opinions of authors expressed in this work do not necessarily state or reflect those of the United States Government, or its contractors, or subcontractors.

Large Plate Experiment of Chloride-induced Stress Corrosion Cracking in Spent Nuclear Fuel Storage Canisters

Spent Fuel and Waste Disposition

Prepared for
U.S. Department of Energy
Spent Fuel and Waste Science and Technology

Andrew J. Duncan
Lisa N. Ward
Emmanuel E. Perez
Thanh-Tam T. Truong
Robert L. Sindelar
Savannah River National Laboratory

EXECUTIVE SUMMARY

This report is the comprehensive description of the completed experiment to evaluate the corrosion behavior of a large section of welded plate material harvested from the Sandia National Laboratories' (SNL) full-size mockup of a spent nuclear fuel (SNF) dry storage canister. The plate was subjected to conditions aggressive to chloride-induced stress corrosion cracking for a total time of 2 years. The details of the establishment of this experiment, and the corrosion results are reported. This work is intended to inform aging management programs for SNF canisters under conditions of extended dry storage.

A "large plate" containing a circumferential weldment from the SNL mockup canister was the test specimen. The knowledge of the salt, temperature, humidity conditions aggressive to cause chloride-induced stress corrosion cracking (CISCC) including the threshold stress intensity factor, K_{ISCC}, were used to setup the experiment. The plate contained a set of seven part-through-wall and through-wall electrical discharge machined (EDM) defects, positioned in the weld residual stress field of the weldment. The weld residual stresses, and the stress intensity of a crack located in the residual stress field were rigorously evaluated previously – the results are replicated in this report for completeness.

A marine salt solution (ASTM D1141) was applied to this plate specimen with an air-brush spray, then dried, and then exposed to a sustained 71-73% RH condition at an ambient room temperature of 22 °C. The experiment ran for a 2-year exposure period (May 2019 to May 2021).

The results show that general corrosion and pitting corrosion in local patches occurred on the plate surface within days of exposure, however, there were no marked visual appearance changes over the balance of the exposure period after the first month. The plate was cleaned, and non-destructive examination using visual test, penetrant test, and ultrasonic test methods were performed. Destructive examination was performed using serial sectioning parallel to the plate top surface on one EDM defect (VP-2).

Small pits (maximum of 300 μm deep) and small cracks (maximum of 44 μm at a depth 3 mm from the top surface of plate) were observed from the VP-2 defect at all depths interrogated beneath the surface of the plate using optical and laser confocal microscopy. There was no correlation between pit size and cracking; and there was no correlation between the (calculated) stress intensity and the incidence and size of the cracks.

The maximum observed CISCC crack growth rate of 22 μm/year is below the lower bound of the 95% confidence interval for the crack growth rate of 36 μm/year at 22 °C from the SNL model. No significant crack growth had occurred.

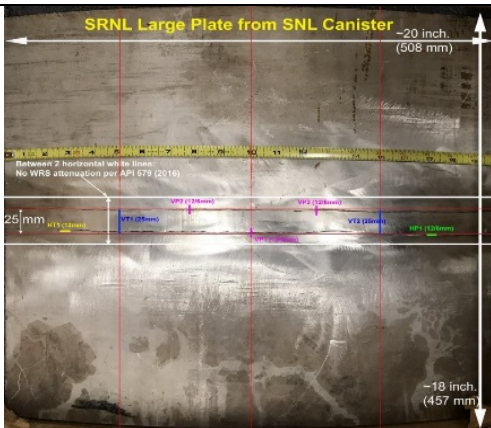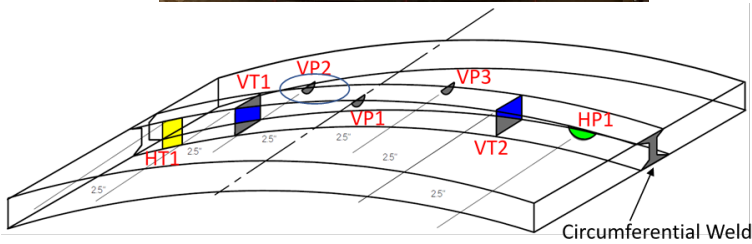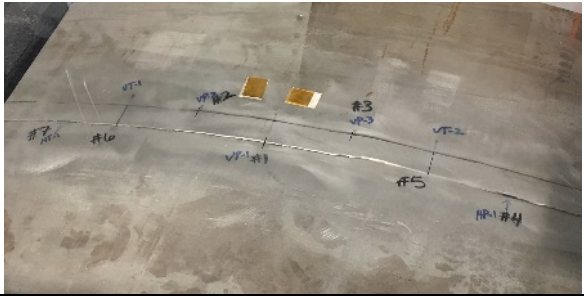The experiment metrics and the results are compiled in Table ES-1 below.

This report fulfills the M3 milestone M3SF-21SR010207082, "Summary Report of the Canister Plate Corrosion Crack Growth Testing" under Work Package Number SF-21SR01020708.
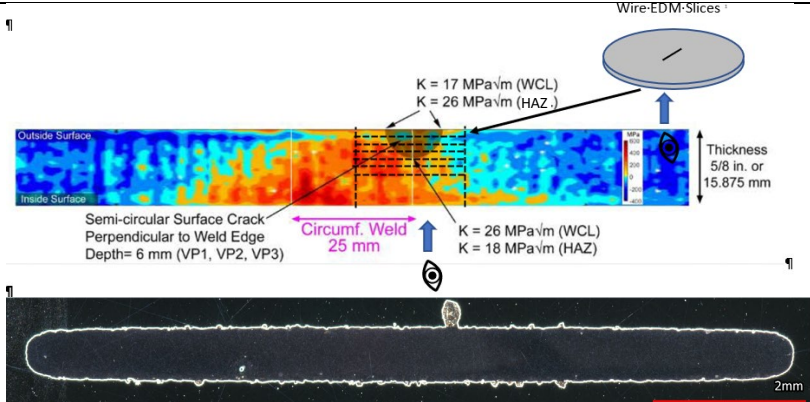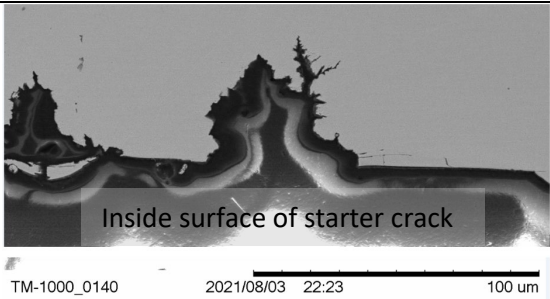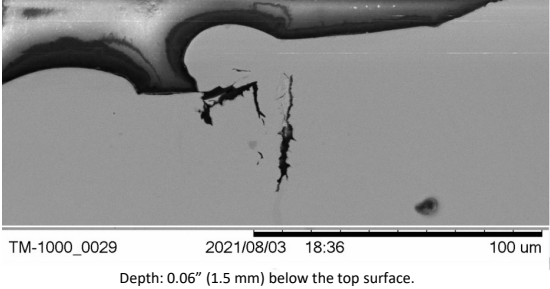
Table ES-1 – Large Plate Experiment Setup and Results

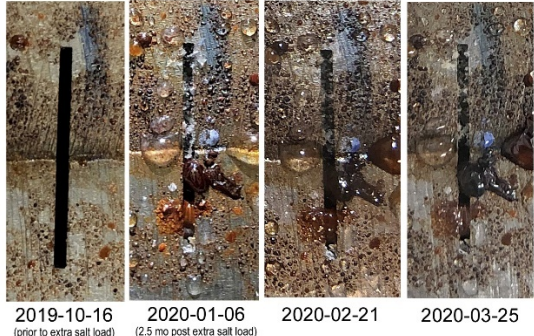| Experiment Metric	Notes	Image
Plate Test Specimen	Dual-certified 304/304L plate, approximately 51×46 cm with thickness 16 mm and weight about 30 kg containing a circumferential weldment. Seven (7) electrical discharge machined defects throughwall and part-throughwall, perpendicular and parallel to the weldment in the residual stress region of the weldment	
Applied Salt Loading onto Plate	2.3 g/cm^2 chloride using ASTM D1141 salt applied in spray and dried on plate prior to exposure to temperature and humidity in an enclosed plexiglass chamber	Estimated Salt Load on Top Surface: 2.3 g/m2 chloride (Dry) (From artificial sea water prepared by ASTM D1141)
Test Start/Stop Dates	May 8, 2019 to May 12, 2021	
Additional Salt Loading onto pre-defect VP2 and HP1	Estimated < 5 g/cm^2 applied September 2019.	
Testing Temperature	22°C - Non-controlled ambient room temperature	
Testing Relative Humidity	71-73% - Controlled with ASTM E 104 salt system in box enclosure	

Experiment Metric	Notes	Image
Visual Test Results	Clear evidence of rusting and staining. The rusting appearance remained essentially unchanged after first month throughout the 2-year exposure period	
Penetrant Test Results	No evidence of SCC at weld toe region (crevice) or at surface out from 7 EDM defects	
Ultrasonic Test Results	Inconclusive with no definitive call of SCC from any of the 7 EDM defects	
Destructive Examination Results	Destructive examination sectioned starter defects and imaged them from bottom surface of the slices. Cracking and Pitting grows out from inside surface of starter defect into the section thickness of the plate.	 LCM (Optical) Micrograph of EDM Notch Sample 2

Experiment Metric	Notes	Image
Maximum Observed Crack Growth Rate	CGR = 0.022 mm/year (0.044 mm maximum SCC crack depth observed after 2-year exposure, and assuming no initiation time) The maximum pit depth observed was 300 μm from inside surface of EDM defect into the section thickness of the plate. The images are at 0.06" (1.5 mm) beneath the top surface of the plate.	 Inside surface of starter crack TM-1000_0140 2021/08/03 22:23 100 um TM-1000_0029 2021/08/03 18:36 100 um Depth: 0.06" (1.5 mm) below the top surface.

ACKNOWLEDGMENTS

This page is intentionally left blank

CONTENTS

LIST OF FIGURES

LIST OF TABLES

ACRONYMS

AMP	Aging Management Program
API	American Petroleum Institute
ASME	American Society of Mechanical Engineers
BLCT	Bolt-load Compact Tension (specimen)
BM	Base metal
BPVC	Boiler and Pressure Vessel Code
CISCC	Chloride-Induced Stress Corrosion Cracking
CGR	Crack Growth Rate
COD	Crack opening displacement
CRIEPI	Central Research Institute of Electric Power Industry (Japan)
CT	Compact Tension Specimen
DAS	Data acquisition system
DOE	US Department of Energy
EDM	Electrical Discharge Machining
EIS	Electrochemical Impedance Spectroscopy
EPRI	Electric Power Research Institute
GW	Guided Wave
HAZ	Heat Affected Zone
ISFSI	Independent Spent Fuel Storage Installation
I-NERI	International Nuclear Energy Research Initiative
JIS	Japanese Industrial Standard
KU	Korea University
LWR	Light Water Reactor
NDE	Nondestructive Examination
NE	Nuclear Energy
NRC	Nuclear Regulatory Commission
PAUT	Phased Array Ultrasonic Test
PL	Pulsed Laser
PNNL	Pacific Northwest National Laboratory
PS	Proof Stress (Stress at 0.2% strain)
PT	Liquid Dye Penetrant Testing

PZT	Piezoelectric Transducer
RH	Relative Humidity
RN	Rating Number
SAW	Submerged arc welding
SCC	Stress Corrosion Cracking
SIF	Stress Intensity Factor
SLDV	Scanning Laser Doppler Vibrometer
SNF	Spent Nuclear Fuel
SNL	Sandia National Laboratories
SRNL	Savannah River National Laboratory
UT	Ultrasonic Test
VT	Visual Inspection
WRS	Welding Residual Stress
XRD	X-ray Diffraction

1. INTRODUCTION

This report describes the experiment to evaluate chloride-induced stress corrosion cracking (CISCC) growth behavior using a large plate harvested from the Sandia National Laboratories' (SNL) mockup canister. The purpose of the experiment was to investigate CISCC growth behavior in an as-fabricated canister weldment as driven by weld residual stress (WRS).

A large section (approximately 51×46 cm with nominal thickness 16 mm and weight about 30 kg), which contains a circumferential weld, was cut from a mockup canister at SNL [1]. Through-wall and part-through-wall (surface) starter cracks, either parallel or perpendicular to the weld, were fabricated with electrical discharge machining (EDM). The stress intensity factor (K) for each machined starter crack under canister welding residual stress was estimated by the American Petroleum Institute (API) 579 procedure [2-4]. Dry salt was applied over these machined cracks (estimated 2.3 grams Cl^-/m^2) and natural deliquescence was allowed to take place at room temperature approximately 22 °C and 73% relative humidity (RH) [5, 6]. The large plate test was initiated May 8, 2019 and completed May 12, 2021 after 2 years exposure. The large plate was taken out of the exposure cell and cleaned for nondestructive examination (NDE) to inspect for stress corrosion cracks that might have initiated and grown from the edges of the starter cracks. The NDE was followed by destructive examination (DE) by serial sectioning from the plate surface of the selected starter defect (into thin slices to reveal potential crack growth and crack morphology. The results are presented in this report and compared to literature CGR test results [7].

The background for this large plate experiment is described in the report issued last year [8].

Sections 2 through 2.5 are mostly replicated from reference 8 so as to provide a complete record of the experiment in this report. Section 2.6 to end of the report is the new results of the examination of the plate using non-destructive and destructive examination.

2. SAVANNAH RIVER LARGE PLATE DEMONSTRATION EXPERIMENT

The CISCC for long-term storage of the SNF canisters is investigated at Savannah River Laboratory with a large stainless steel plate (dual certified 304/304L) harvested from the full-size mockup canister at Sandia National Laboratories. The canister plate chemical composition [1] and the tensile properties[1] are shown in Tables 1 and 2, respectively.

---

[1] Enos, David G. to Sindelar, R. L., email communication, May 5, 2016 (Attachment: "Weld parameters.xlsx").

Table 1. Material Chemical Composition for Sandia mockup canister (wt.%) [1]

Materials	C		Co	Cr	Cu	Mn	Mo	N	Ni	P	S	Si
Base Metal 304/304L	0.0223		0.1865	18.1000	0.4225	1.7125	0.3180	0.0787	8.0270	0.0305	0.0023	0.2550
Weld Filler Lot 1 308L	0.014		—	19.66	0.16	1.70	0.11	0.058	9.56	0.025	0.010	0.39
Weld Filler Lot 2 308L	0.0012		—	19.71	0.192	1.730	0.071	0.053	9.750	0.024	0.012	0.368

Table 2. Sandia Mockup Canister Plate Tensile Properties (Pre-fabrication)

0.2% Yield Stress	Tensile Strength (UTS)	Elongation in 50.8 mm (2 inch.) Gauge	Reduction in Area (RA)	Hardness (RB)
37.87 ksi 261 MPa	86.6 ksi 597 MPa	62.5%	66.43%	81.5

As shown in Figure 1, the Savannah River large plate was sectioned through a region of the canister that contains a circumferential weld and has a planar dimension of 51×46 cm (20×18 inch.) with a nominal thickness of 16 mm (⅝ inch.) and its weight is approximately 30 kg. The SRNL large plate exposure to temperature and controlled humidity conditions was initiated May 8, 2019 and completed May 12, 2021.
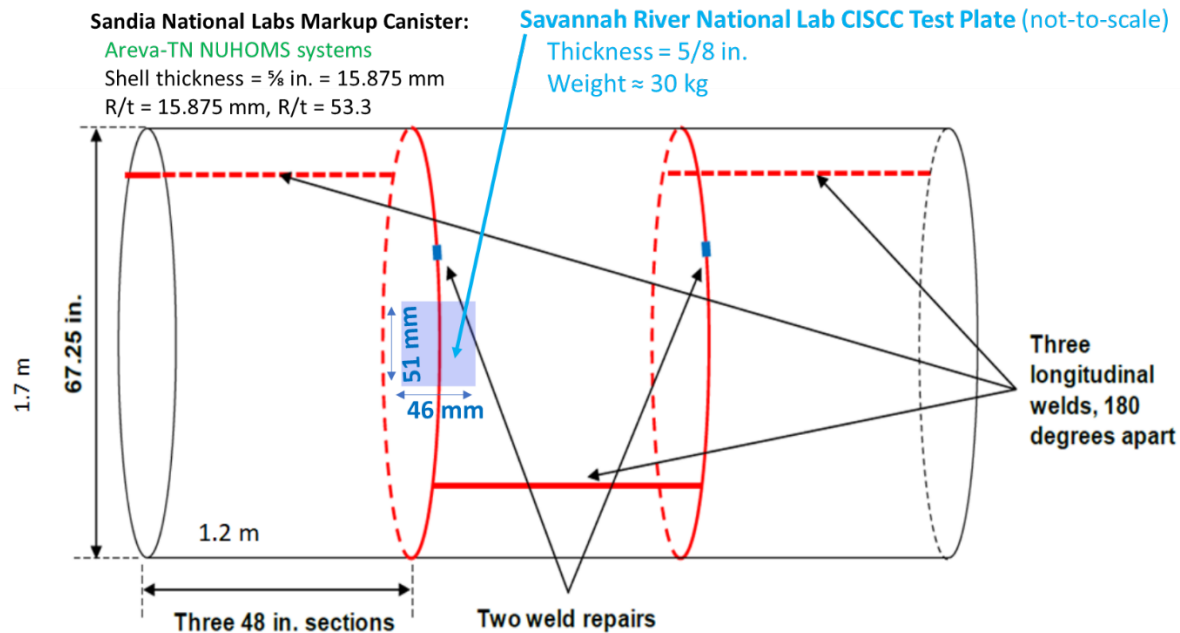
Figure 1. A sketch of the full size mockup canister showing the fabrication welds and the representative location where the SRNL large plate was harvested

2.1.   Welding Residual Stress

The SNF storage and transportation canisters are not required to have post-weld heat treatment after fabrication to relieve the WRS. Under certain corrosive environmental conditions, such as in the chloride-rich coastal regions where the canisters are stored, the WRS could become the mechanical driving force to cause SCC. This phenomenon has been demonstrated in similar large plate tests for welded A285 and A537 carbon steels used to construct the Savannah River high-level nuclear waste tanks [9-11] and the results were consistent with field experience.

To facilitate structural integrity assessment as required in the AMP for SNF canisters, the WRS distributions have been determined experimentally at SNL [1]. For a circumferential weld that is associated with the current Savannah River large plate test, the SNL WRS results are summarized in Figure 2, in which the black curves represent the average of the experimental (measured) values [1], and the red curves are the 4th-order polynomial curve fitting that is needed to facilitate stress intensity factor (SIF) calculations with API 579 [2, 3] (or other similar national or international consensus codes for the industry). The 4th-order polynomial fit reported here was obtained by Korea University under DOE I-NERI/USA-ROK program [12]. These residual stresses were also determined using the finite element method [13] by simulating the actual welding procedure documented in a previous report [1] and are in good agreement with the experimental results. The designations of these welding residual stresses are shown in Figure 3, where RS2 is the WRS component parallel to the weld and tends to open an axial crack, and RS3 is the WRS perpendicular to the weld and is responsible for opening a circumferential crack.
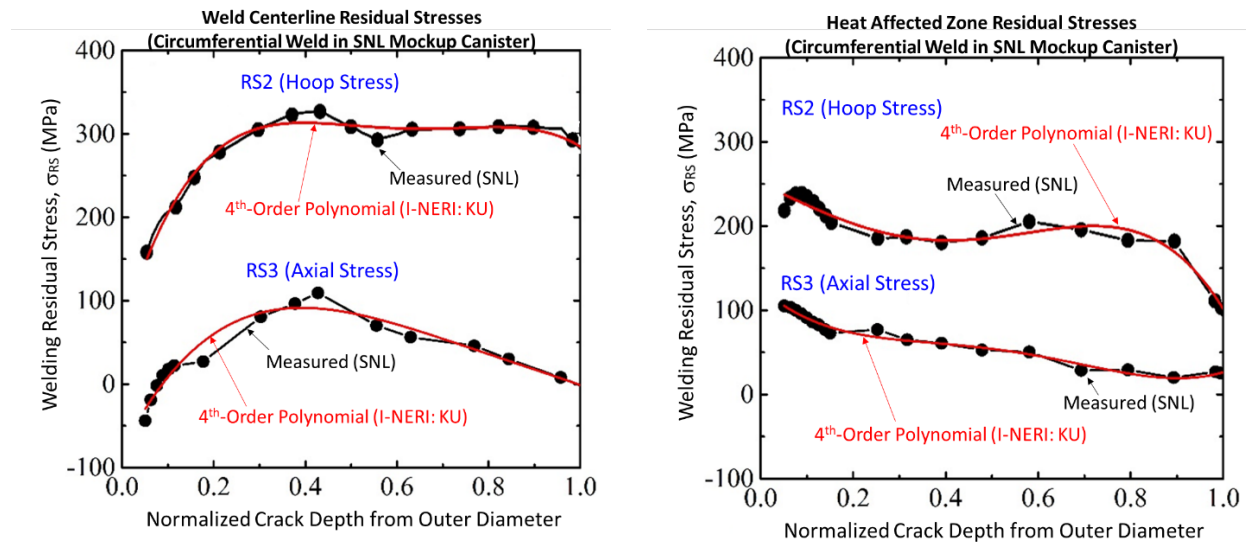
Figure 2. Welding residual stresses associated with the canister circumferential weld. The Weld Centerline and the Heat Affected Zone Residual Stresses were measured at the approximate center of the weld, and at 4 mm from the weld toe (fusion line) into the base material, respectively [1]
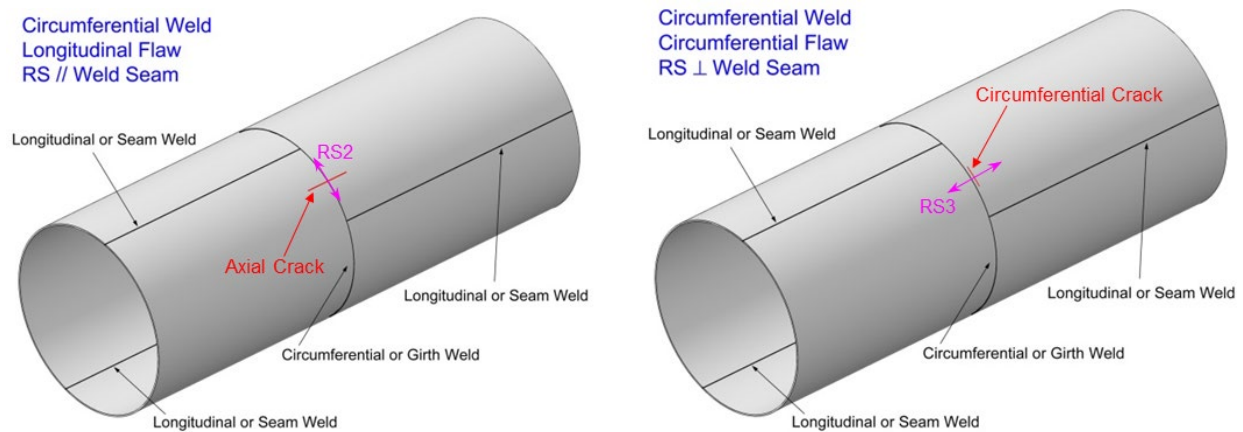
Figure 3. Designations of residual stresses (RS2 and RS3) for a circumferential weld in a canister

The sizes of the experimental large plates sectioned from the Sandia mockup canister were carefully determined from a series of finite element calculations to minimize WRS redistribution or relief due to cutting[2]. In a separate study at Oak Ridge National Laboratory [14], neutron diffraction was used to determine the remaining WRS in their large plate also from the same mockup canister but with an axial weld. Their experimental data confirmed that most of the as-welded residual stresses were retained in the sectioned plate. Therefore, it is reasonable to assume that the residual stresses in the SRNL large plate were not altered significantly and are similar to those in Figure 2.

2.2.   Starter Cracks or Defects

Starter cracks or defects (aka seed cracks or machined cracks) were introduced to the large plate in the weld region by EDM. They are intended to create a favorable fracture environment for a stress corrosion crack to initiate and grow under WRS loading. This concept is similar to the fracture toughness test where an initial notch/crack is machined into the specimen (e.g., a compact tension specimen or a single edge notched bend specimen), and it is a standard method to determine the threshold stress intensity factor (K_{ISCC}), below which the SCC is unlikely to occur.

There are seven starter cracks built in the SRNL large plate (Figures 4). The designations and descriptions of these EDM starter cracks are:

Type (a) VT1, VT2: through-wall crack across the weld, crack length = 25 mm;

Type (b) HT1: through-wall crack parallel to the weld edge, crack length = 12 mm;

---

[2] Bryan, C. to Sindelar, R. L., email communication, August 14, 2018.

Type (c) VP1, VP2, VP3: semicircular part-through-wall crack (surface crack) perpendicular to the weld edge, crack length= 12 mm and crack depth = 6 mm;

Type (d) HP1: semicircular part-through-wall crack (surface crack) parallel to the weld edge, crack length= 12 mm and crack depth = 6 mm.

The starter crack layout and orientation is schematically shown in Figure 4. Each type of the EDM crack configuration is shown in Figure 5. When these cracks are overlaid over the contour map of the residual stress parallel to the circumferential weld [1], the WRS loading of these cracks can be seen in Figure 6. The starter crack tips are located in the weld/HAZ region. Note that the stress contour in Figure 6 only applied to the starter cracks that are perpendicular to the weld (i.e., VT1, VT2, VP1, VP2, and VP3).
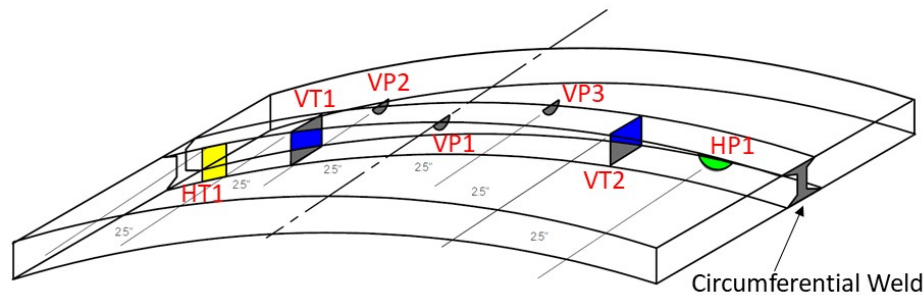
Starter Crack Description (total 7 EDM cracks):
VT1, VT2: Through-wall crack across the weld.
          Crack length= **25 mm**
HT1: Through-wall crack parallel to the weld edge.
     Crack length= **12 mm**.
VP1, VP2, VP3: Semi-circular Part-through-wall crack perpendicular to the weld edge.
               Crack length= **12 mm** and crack depth = **6 mm**
HP1: Semi-circular Part-through-wall crack parallel to the weld edge.
     Crack length= **12 mm** and crack depth = **6 mm**

Figure 4: Starter crack layout and orientation in the large plate
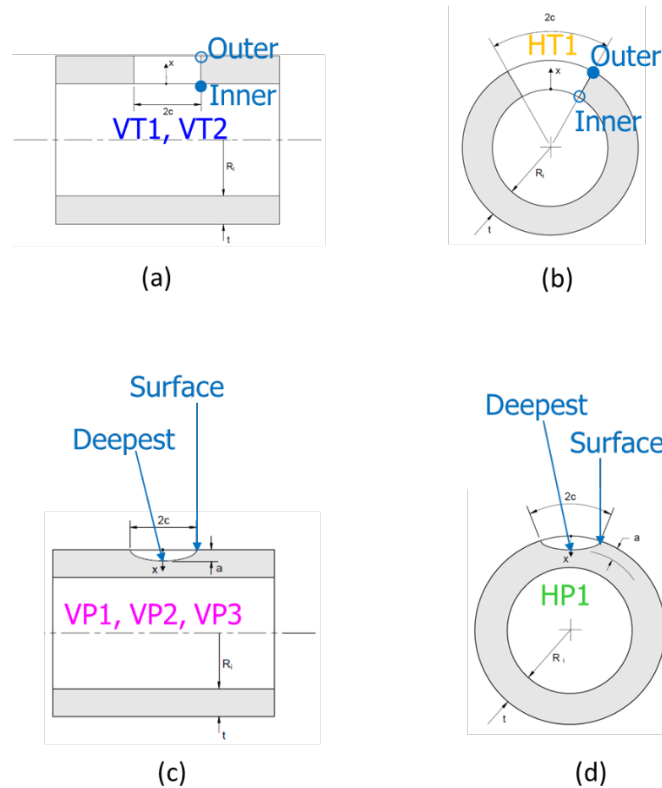
Figure 5. Large plate starter crack configurations: Type (a) VT1, VT2: through-wall crack across the weld; Type (b) HT1: through-wall crack parallel to the weld edge; Type (c) VP1, VP2, VP3: semicircular ($a = c$) part-through-wall crack perpendicular to the weld edge; and Type (d) HP1: semi- circular ($a = c$) part-through-wall crack parallel to the weld edge
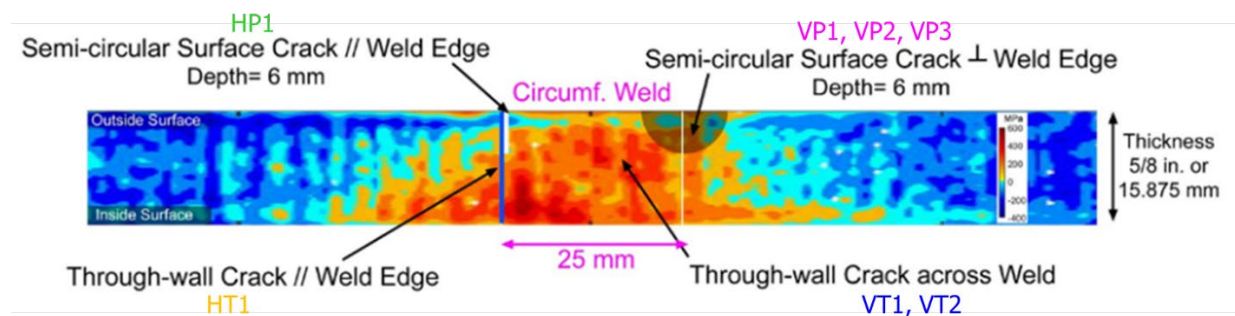
Figure 6. Large plate starter crack design as viewed from plate cross-section through the circumferential weld (superimposed over the contour map for welding residual stress parallel to the weld [1])

The through-wall cracks (VT1, VT2, and HT1) were fabricated with EDM wires of 0.25 mm (0.010 in.) diameter (65% copper and 35% zinc). The resulting width (burn gap) on the plate surface (corresponding to the outer surface of the canister) is approximately 0.43 mm by measurement. For the semicircular, part-through-wall cracks (VP1, VP2, VP3, and HP1),

graphite ram EDM electrodes with width 0.51 mm (0.02 in.) were used. The machined starter crack width on the plate surface is about 0.81 mm.

2.3.   Experiment

Artificial sea salt was prepared by following the procedure recommended by ASTM D1141, then deposited on the outer surface of the plate in the welded region with an air brush. The estimated salt load on the plate top surface was 2.3 g/m^2 chloride (dry). The salt coating procedure, as outlined in ASTM G41, "Standard Practice for Determining Cracking Susceptibility of Metals Exposed under Stress to a Hot Salt Environment," was used to create an evenly distributed salt layer over the plate surface. Figure 7 shows the large plate after salt spray and drying, ready for placing inside the test cell.
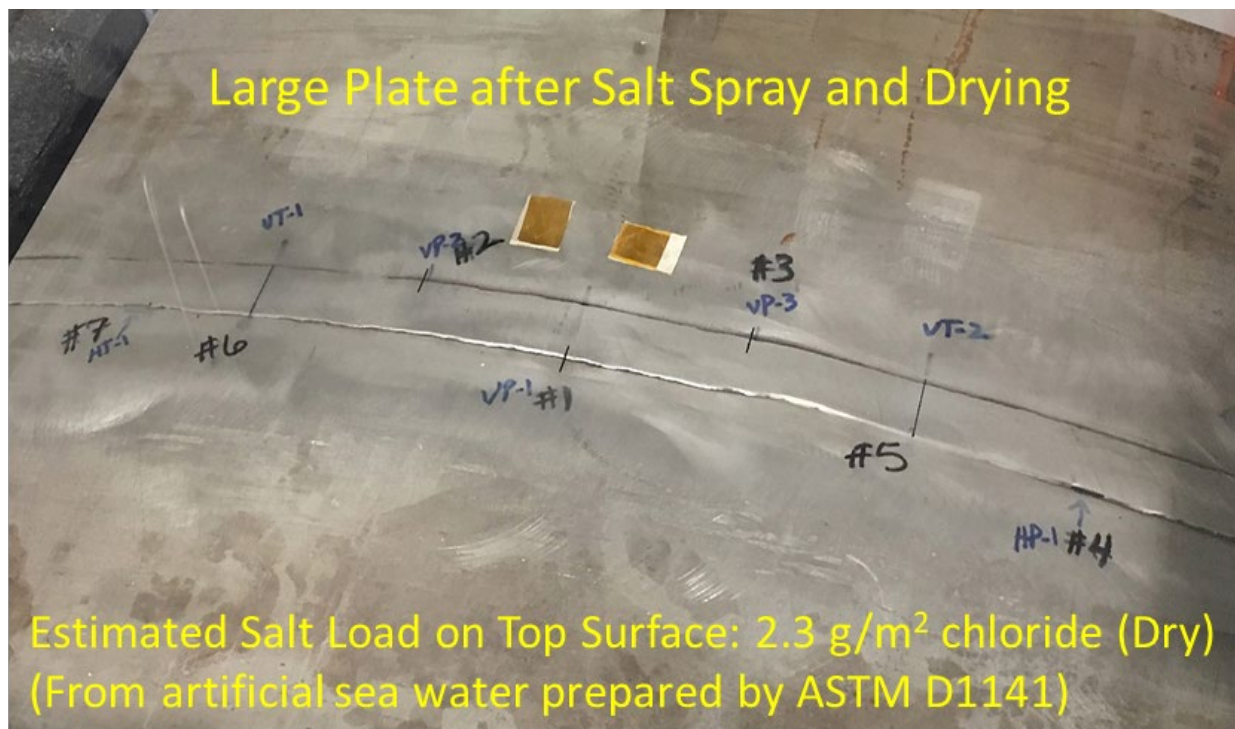
Figure 7. Large plate with EDM starter cracks after salt spray and drying

A transparent polycarbonate (LEXAN™) test cell with an outside dimension of 56×53×15 cm with wall thickness 12.7 mm (0.5 in.) was constructed to house the large stainless steel plate which is supported by a riser over a salt bed with saturated NaCl. Based on ASTM E104, a constant 73% RH environment would be maintained inside the water-tight test cell at room temperature typically 22 °C.

Initially, seven Phased Array Ultrasonic Test (PAUT) wedges and transducers were mounted on the salt-free surface of the plate (or the concave side of the plate corresponding to the inner surface of the canister) for on-line monitoring of crack growth. These sensors have been since removed due to excessive noise preventing satisfactory measurements. Figure 8 illustrates the overall experimental setup and Figure 9 shows the closeup of the salt tray that is used to maintain a constant RH environment by following ASTM E104, "*Standard Practice for Maintaining Constant Relative Humidity by Means of Aqueous Solutions.*"

The large plate was exposed to a CISCC environment in 73% RH at room temperature (~22 °C) from May 2019 through May 2021.
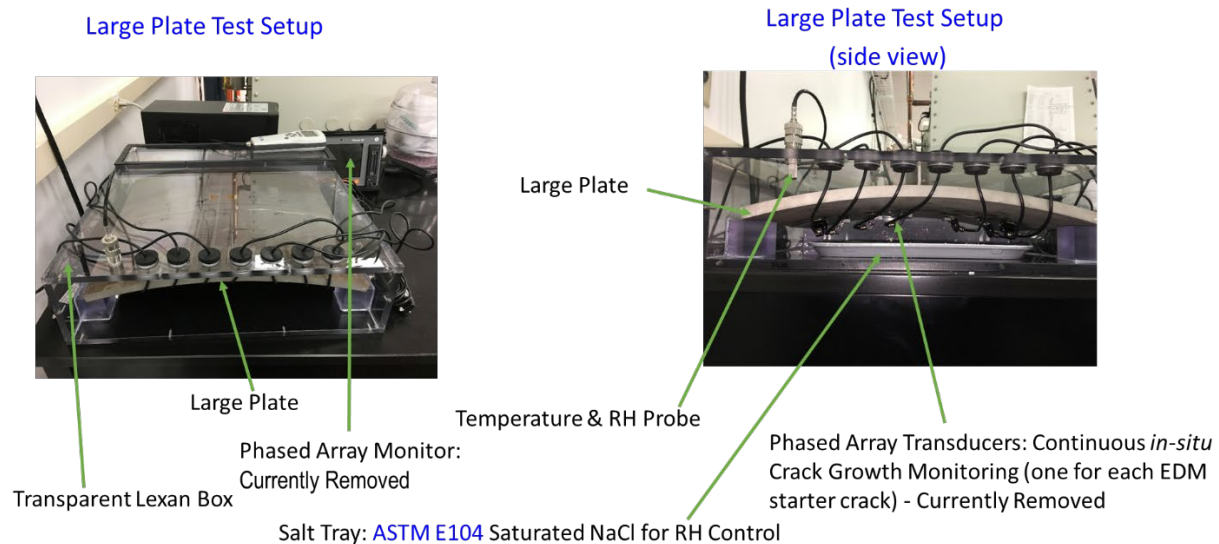
Figure 8. Experimental setup of the large plate CISCC test under naturally deliquescing sea salt at room temperature and 73% RH (PAUT wedges have been removed)
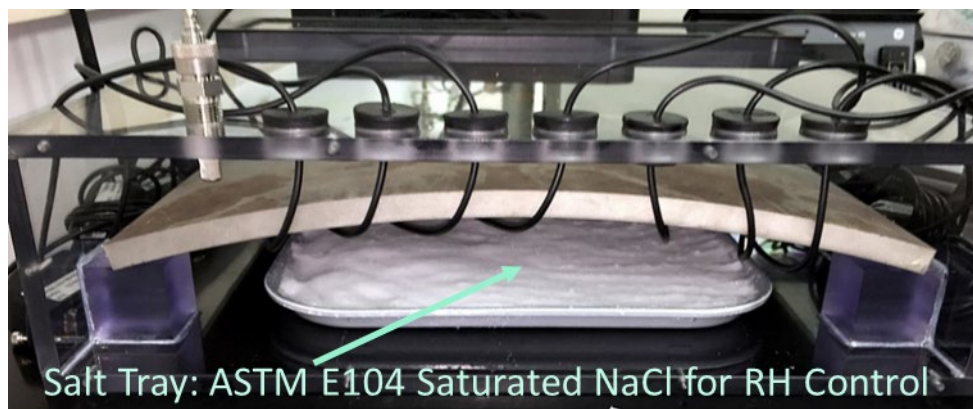
Figure 9. The NaCl salt tray under the large plate for maintaining a constant relative humidity in the test cell

2.4.   Experimental Observations

The test was initiated on May 8, 2019. The temperature and RH reached equilibrium within one day. The initially dry salt film originally covered the plate surface turned into numerous liquid droplets in a few hours, similar to the "big plate" tests conducted at Sandia National Laboratories [8]. This indicated that the natural deliquescence has taken place.

2.4.1. Initial Exposure (5 Months)

The SRNL large plate test has been periodically examined for CISCC and documented with digital images for each starter crack. The evolution of the starter cracks and their immediate vicinities, observed from May 9 to October 16, 2019, is shown in Figure 10. As shown in Figure 10, general corrosion is progressively developed, especially along the weld and the base metal interface.
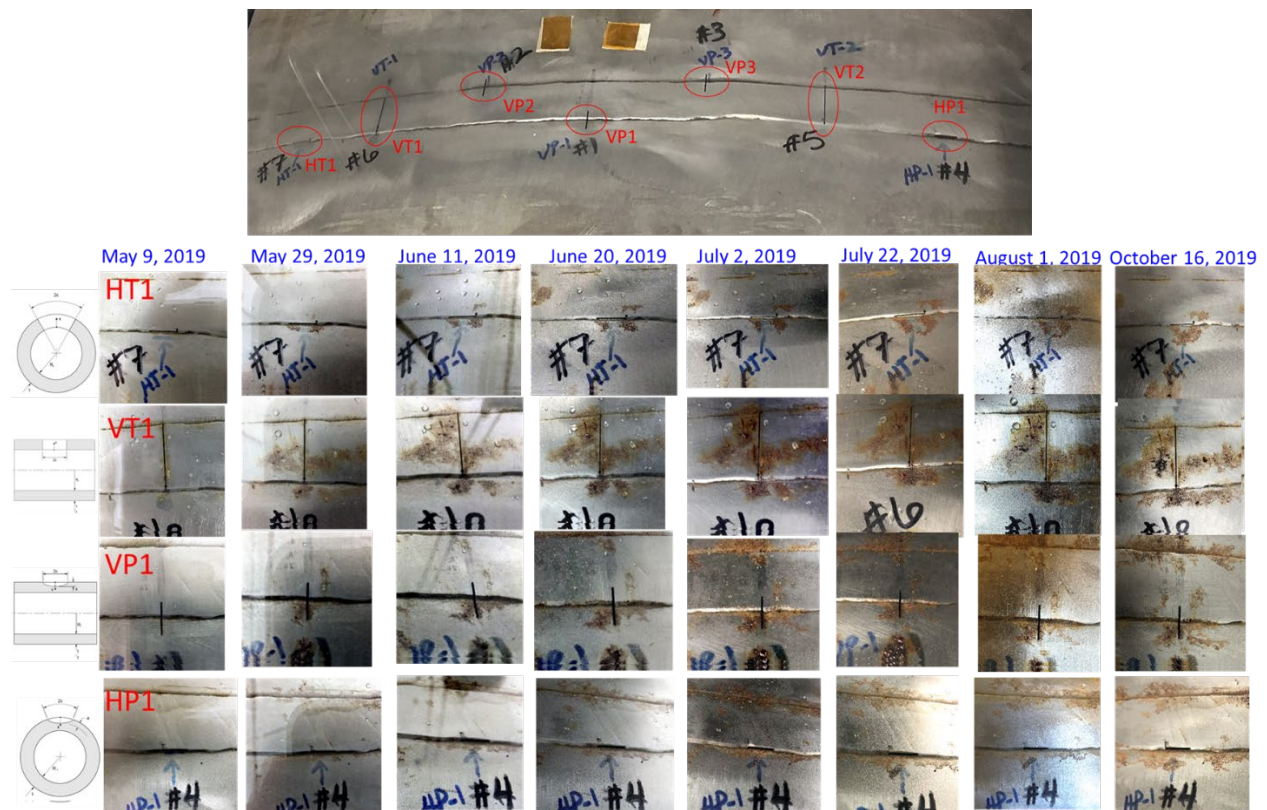
Figure 10. Evolution of chloride-induced corrosion near starter cracks during 5 months of exposure at room temperature about 22°C and 73% RH

2.4.2. Test Augmented with Elevated Chloride Concentration

Because no cracking was observed after 5 months of exposure with the initial salt load of 2.3 grams Cl$^-$/m^2 on the plate surface, two starter cracks (VP2 and HP1) were selected to receive additional salt load, where VP2 is a semicircular surface crack perpendicular to the weld, and HP1 is a semicircular surface crack parallel to the weld edge. The original crack lengths are both 12 mm on the plate surface. As seen in Figure 11, these two cracks were isolated with putty material (yellow) from the other starter cracks and the extra salt was applied to the enclosed areas on October 24, 2019). The deliquesced salt brine droplets can be seen in Figure 11.
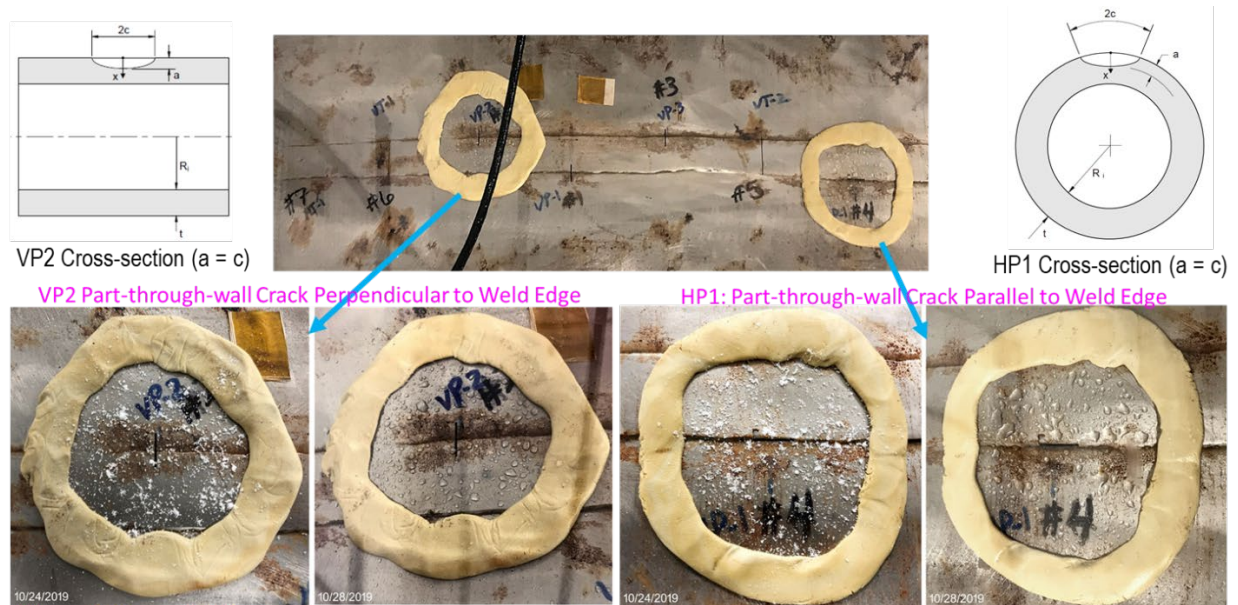
Figure 11. Additional salt applied to selected starter cracks (VP2 and HP1)

Figure 12 shows the corrosion activities of VP2 from October 16, 2019 (about a week before the extra salt was applied) through March 25, 2020. Most of the corrosion products appear to be highly concentrated with iron. A very small spot with light-colored, crack-like morphology seemed to form at the lower crack tip across the crack opening, but it turned out to be a small salt cake or crystal that has been broken up.
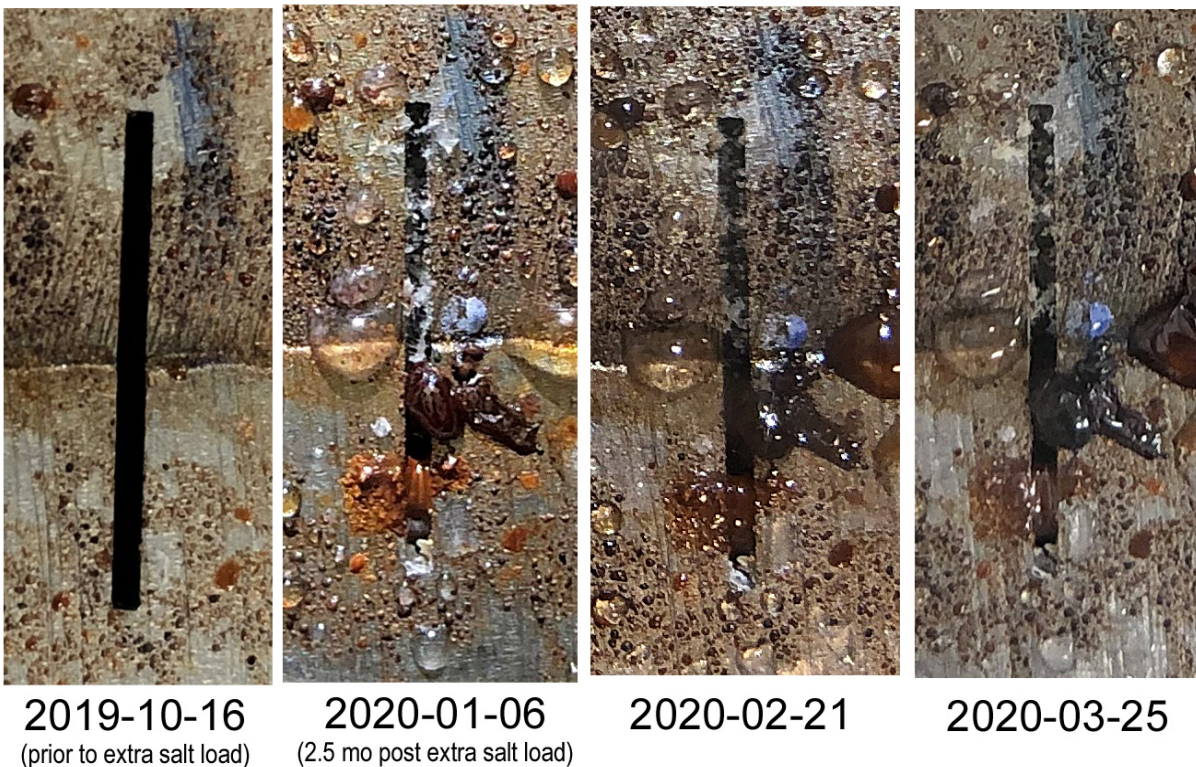
Figure 12. Closeup view of corrosion evolution of a semicircular surface crack VP2 after additional salt was applied (original crack length is 12 mm and is perpendicular to the weld)

2.4.3. Evolution of General Corrosion

A comparison of general corrosion in the weld region across the width of the entire large plate from May 9, 2019 (test initiation date) through February 21, 2020 is shown in Figure 13. The corrosion pattern appears to be stabilized quickly (sometime between May and October 2019). Even with extra salt applied to the two starter cracks on October 2019, it seems that the appearance of general corrosion was not affected (Figure 13). Of course, in the very close vicinities around those two starter cracks with extra salt load, the general corrosion remains relatively active (see VP2 in Figure 12).

Figure 13. Evolution of general corrosion on the large plate in weld region

2.5.   Propensity of CISCC in Large Plate with Starter Cracks

The Mode I stress intensity factor (K_I) is typically used as an indication for an existing crack whether it will grow in tensile opening mode under the external or internal loads. In the case of SCC, a threshold stress intensity factor, K_{ISCC}, may exist, such that crack growth can only take place when $K_I \geq K_{ISCC}$. The value of K_{ISCC} is experimentally determined and it is regarded as an environmentally dependent material property.

2.5.1. Stress Intensity Factor Calculation Procedure

For the current SRNL large plate testing under an exposure condition at room temperature of 22 °C and 73% RH with 2.3 grams Cl^-/m^2 of salt on the plate surface, the only loading is the welding residual stresses due to fabrication of the canister. No external loads are applied. Note that for a circumferential weld as in this large plate, only the WRS parallel to the weld (RS2) and that perpendicular to the weld (RS3) are relevant. The API 579 Fitness-for-Service procedure is used to evaluate stress intensity factor K_I for each of the starter crack (see Figure 3-Figure 6): The first step is to approximate the measured through-thickness WRS by a 4th order polynomial, then apply the coefficients of the 4th-order polynomial to the API equations in Annex C of the 2007 edition [2] or Annex 9C in the 2016 edition [3]. The detailed procedure is described below.

(1) Curve fitting of the fourth-order polynomial
Equation (1) is used to curve fit the WRS (σ) measured by Sandia National Laboratories [1] (see Figure 2):

$$\sigma(x) = \sigma_0 + \sigma_1 \left(\frac{x}{t}\right) + \sigma_2 \left(\frac{x}{t}\right)^2 + \sigma_3 \left(\frac{x}{t}\right)^3 + \sigma_4 \left(\frac{x}{t}\right)^4 \tag{1}$$

where σ_i (i=0 to 4) are the coefficients of the 4th-order polynomial, t is the canister wall thickness, and x is the through-wall coordinates with x= 0 at the inside dimeter (ID) of the canister for through-wall cracks or x=0 at the outer diameter (OD) for the outside part-though-wall surface cracks (see the coordinate system in Figure 5, or its definition in API 579 [2,3]). The values of σ_i have been determined by Korea University under I-NERI/USA-ROK program [12] and are listed in Table 3.

Table 3. Coefficients of the 4th-Order Polynomial to Approximate Welding Residual Stress

Seed Crack	Crack Location	x=0 Location	σ_0 (MPa)	σ_1 (MPa)	σ_2 (MPa)	σ_3 (MPa)	σ_4 (MPa)
VT1, VT2	WCL	ID	283	347	-1701	3310	-2169
	HAZ		100	902	-2746	3136	-1142
VP1, VP2, VP3	WCL	OD	69	1803	-4787	5367	-2169
	HAZ		249	-249	-191	1432	-1142
HT1	WCL	ID	-1	191	-80	361	-550
	HAZ		27	-162	1077	-1751	936
HP1	WCL	OD	-79	1086	-2298	1840	-550
	HAZ		127	-484	1442	-1994	936

WCL: Weld Centerline
HAZ: Heat Affected Zone

Seed Crack Description:
VT1, VT2: Through-wall crack, longitudinal direction, perpendicular to circumferential weld.
VP1, VP2, VP3: Surface crack on outer diameter, longitudinal direction, perpendicular to circumferential weld.
HT1: Through-wall crack, circumferential direction, parallel to circumferential weld.
HP1: Surface crack on outer diameter, circumferential direction, parallel to circumferential weld.

(2) Stress intensity factor calculation:
As outlined by the API 579-1/ASME FFS-1 [2, 3], the stress intensity factor for a through-wall crack in a cylindrical shell structure (such as VT1, VT2, or HT1) is expressed by

$$K_I = \left[\{\sigma_m + p_c\} G_0 + \sigma_b (G_0 - 2G_1) \right] \sqrt{\pi c}$$

where σ_m is the membrane stress component of the loading, σ_b is the bending stress component, p_c is the crack face pressure and is zero in the current large plate case, and the influence coefficients G_0 and G_1 are tabulated in API 579 [2, 3] for each crack orientation (axial or circumferential) and are a functions of t/R_i (i.e., the ratio of canister wall thickness to canister inside radius). For the equivalent membrane and bending stresses in terms of the 4th-order polynomial formulation:

$$\sigma_m = \sigma_0 + \frac{\sigma_1}{2} + \frac{\sigma_2}{3} + \frac{\sigma_3}{4} + \frac{\sigma_4}{5}$$

$$\sigma_b = -\frac{\sigma_1}{2} - \frac{\sigma_2}{2} - \frac{9\sigma_3}{20} - \frac{6\sigma_4}{15}$$

For a part-through-wall crack without (local) crack face bending, such as the starter crack VP1, VP2, VP3, or HP1, the general expression in API 579 [2, 3] is

$$K_I = \left[G_0 (\sigma_0 + p_c) + G_1 \sigma_1 \left(\frac{a}{t}\right) + G_2 \sigma_2 \left(\frac{a}{t}\right)^2 + G_3 \sigma_3 \left(\frac{a}{t}\right)^3 + G_4 \sigma_4 \left(\frac{a}{t}\right)^4 \right] \sqrt{\frac{\pi a}{Q}}$$

Again, σ_i (i=0 to 4) are the coefficients of the 4th-order polynomial, p_c is the crack face pressure and is zero in the current large plate case, and G_i (i=0 to 4) are influence coefficients that are tabulated in API 579 [2, 3] for each crack orientation (axial or circumferential) and are functions of t/R_i, a/c, and a/t (c is the half crack length of the semi-elliptic surface crack, a is the crack depth, and t is the canister shell thickness).

2.5.2. Stress Intensity Factor Calculation Results

Both sets of welding residual stresses at the weld centerline (WCL) and at the HAZ (Figure 2) were used in calculating stress intensity factors. The experimental data were obtained at Sandia National Laboratories [1] and the 4th-order polynomial curve fitting was performed at Korea University [12].

The SIF solutions for the through-wall axial starter cracks across the circumferential weld (VT1 and VT2) are tabulated in Table 4 and are labelled in Figure 14 at the crack tips where they were calculated. The contour map in Figure 15 represents the WRS parallel to the weld [1]. This stress component is responsible for opening the starter cracks VT1 and VT2. Figure 14 also includes the actual images of VT1 and VT2 after 9 months of exposure. Stress corrosion cracking has not been observed at the crack tips.

Table 4. Stress Intensity factors for starter cracks VT1 or VT2
(Axial through-wall crack: Half crack length c = 12.5 mm)

Welding Residual Stress	Crack Tip Location	Stress Intensity Factor (MPa√m)
Weld Centerline	Outside Surface	51.6
	Inside Surface	64.3
Heat Affected Zone	Outside Surface	46.1
	Inside Surface	33.3
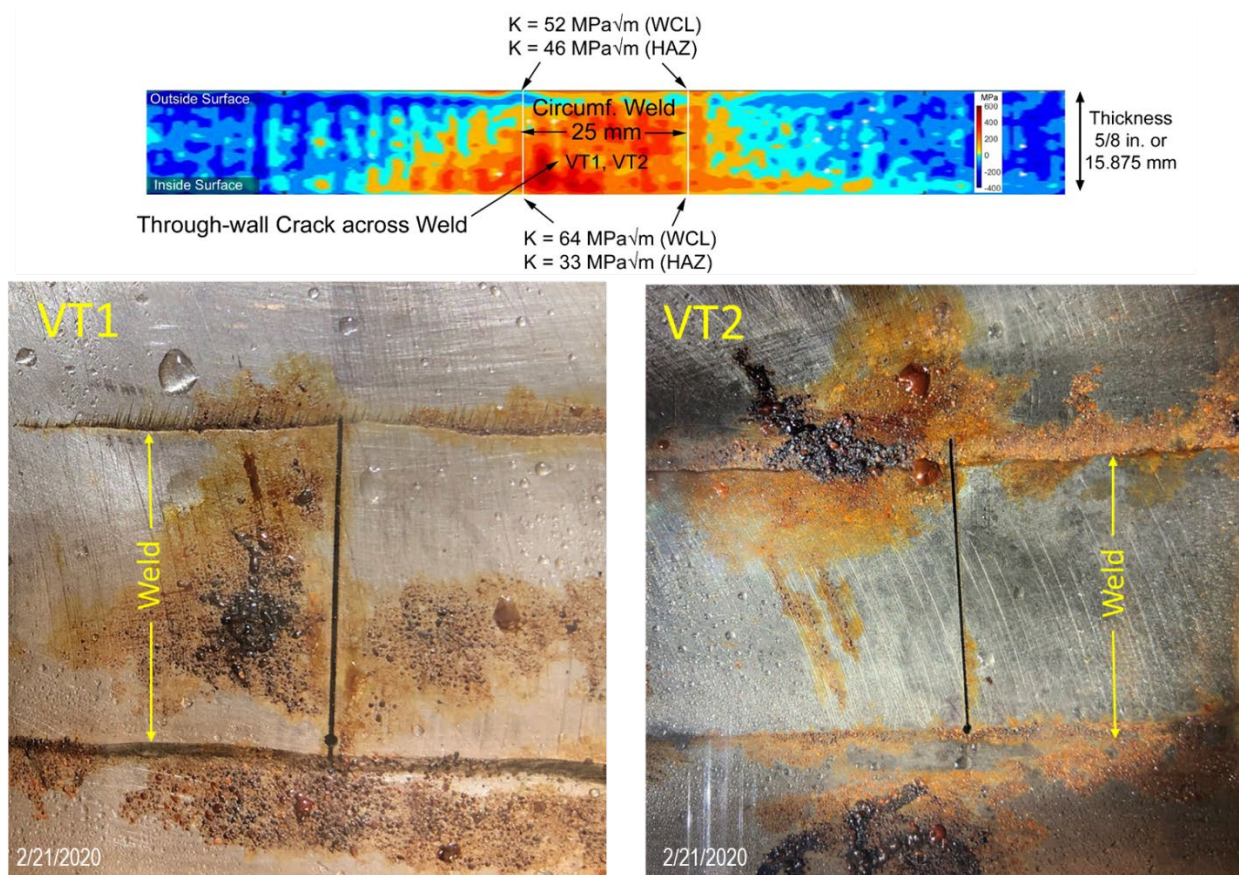
Figure 14. Stress intensity factor solutions for the starter crack VT1 or VT2 and the images of these cracks after 9.5 months of exposure (VT1 and VT2 are through-wall cracks across the weld)

Likewise, the SIF solutions for the part-through-wall axial surface cracks perpendicular to the weld (VP1, VP2, and VP3) are tabulated in Table 5 and labelled in Figure 14. The images after 9months of exposure condition can also be seen in Figure 15. For starter cracks parallel to the weld (HP1: part-through-wall and HT1: through-wall), their SIF solutions are tabulated in Tables 6 and 7 and labelled in Figure 16, which also shows the starter crack images after 9 months of exposure. Stress corrosion cracking has not been observed for any of the starter cracks.

Table 5. Stress Intensity factors for starter cracks VP1, VP2, or VP3
(Axial surface crack: Half crack length a = Crack depth c = 6 mm; Semicircular)

Welding Residual Stress	Crack Tip Location	Stress Intensity Factor (MPa√m)
Weld Centerline	Deepest Point	26.0
	Surface Point	16.9
Heat Affected Zone	Deepest Point	18.3
	Surface Point	26.4
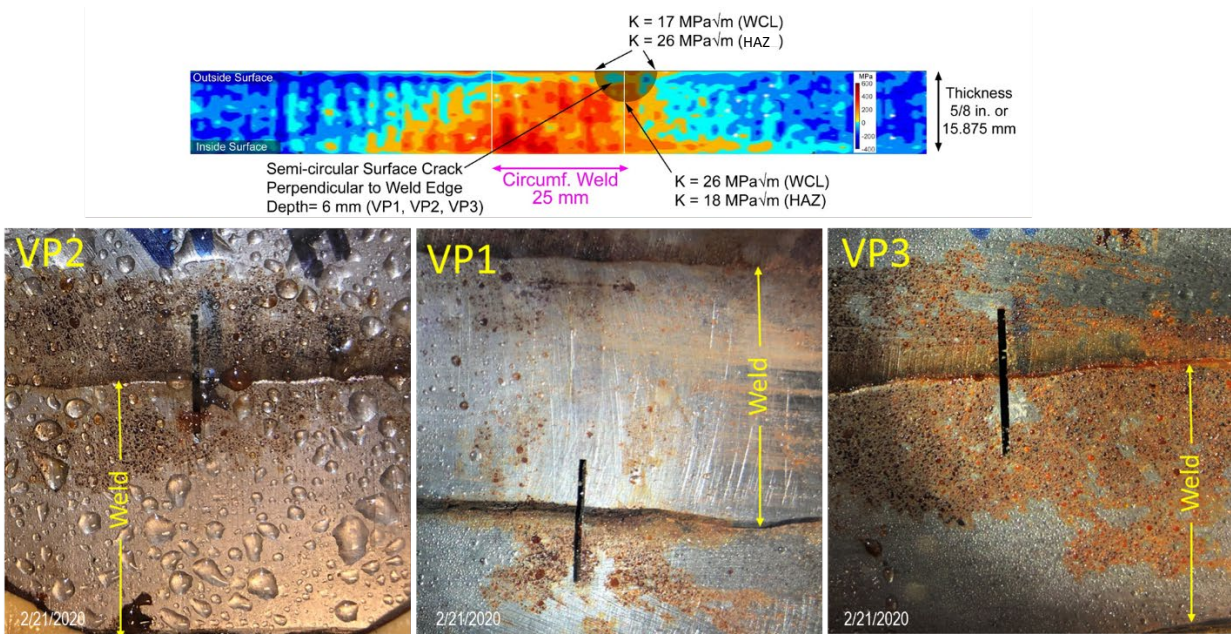
Figure 15. Stress intensity factor solutions for the starter crack VP1, VP2, or VP3 and the images of these cracks after 9.5 months of exposure (VP1, VP2, and VP3 are semicircular part-through-wall surface cracks perpendicular to the weld)

Table 6. Stress Intensity factors for starter crack HP1
(Circumferential surface crack: Half crack length *a* = Crack depth *c* = 6 mm; Semicircular)

Welding Residual Stress	Crack Tip Location	Stress Intensity Factor (MPa√m)
Weld Centerline	Deepest Point	5.6
	Surface Point	-3 (Crack Tip Closure)
Heat Affected Zone	Deepest Point	7
	Surface Point	12

Table 7. Stress Intensity factors for starter cracks HT1
(Circumferential through-wall crack: Half crack length *c* = 12 mm; Semicircular)

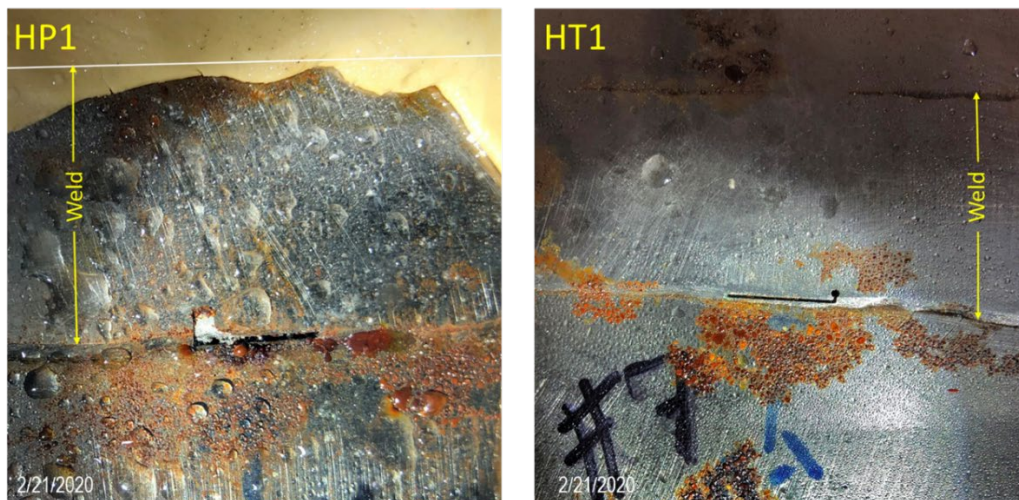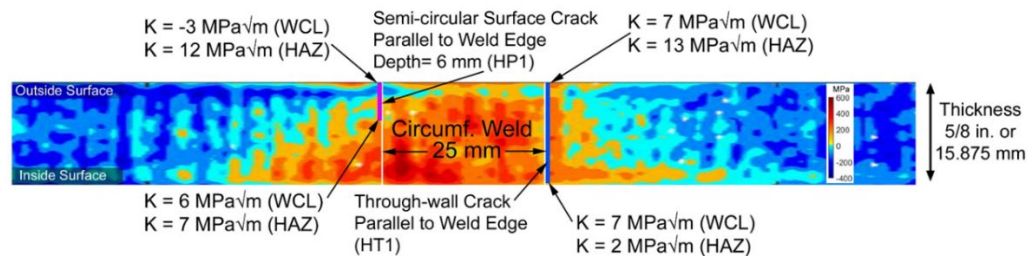| Welding Residual Stress	Crack Tip Location	Stress Intensity Factor (MPa√m)
Weld Centerline	Outside Surface	6.5
	Inside Surface	6.7
Heat Affected Zone	Outside Surface	13.3
	Inside Surface	1.9

Figure 16. Stress intensity factor solutions for the starter cracks HP1 and HT1, and the images of these cracks after 9.5 months of exposure (HP1 is a semicircular part-through-wall surface cracks parallel to the weld; and HT1 is a through-wall crack parallel to the weld)

2.5.3. Propensity of CISCC in Atmospheric Conditions of the Large Plate Test

This section considers existing experimental data of CGR for typical SNF canister stainless steels in chloride-rich environments to provide insight and expectation for the SRNL large plate test.

Natural exposure tests for stainless steels 304, 304L, and 316(LN) were conducted on Miyakojima (Miyako Island), which is one of the most corrosive areas in Japan [15,16]. Three-point bend specimens with thickness of 10 mm, each containing either a 3 mm deep part-through-plate precrack across the width, or a 3mm deep semicircular surface precrack. The specimens were loaded to 0.4 or 0.8 proof stress (PS). Both direct exposure and under glass method were used with average sample surface temperatures at 26.7 and 26.6 °C, respectively. The average relative humidity on the island is 80% (varying between 73% in January and 86% in June [17]). As seen in Figure 18, the experimentally determined CGRs for Type 304 base metal and weld were approximately in the order of 6×10^{-12} m/s, with the K_I loading range between 0.6 to 9 MPa√m.

Accelerated tests were also conducted for the base metal and weld of Type 304 stainless steel by Kosaki [15, 16] at 60 °C and 95% RH using the same specimen design as in the Miyakojima natural exposure tests. The specimens were exposed to NaCl steam mist environment with saturated NaCl concentrated on the specimen surface. The resulting CGRs for Type 304 base metal using semicircular precracked specimens are about 9.3×10^{-10} m/s [13, 14] and the SIF loading range is between 2 and 20MPa√m³, as shown in Figure 19. Also included in Figure 19 are the recent Korea University test data using S30400 stainless steel [18, 19]. The test results were obtained by immersing the specimens in 5 % salinity artificial seawater at 50 °C. Because standard ASTM compact tension specimens were used in the KU tests, higher SIF loading was achieved and K_I was between 15.3 and 23.2 MPa·√m, as shown in Figure 19. The CGRs determined from the immersion test at 50 °C are about 1×10^{-10} m/s, which is one order of magnitude less than the Kosaki data obtained at 60 °C. For comparison purpose, the S31603 test data obtained by Tani et al. [20] at 50 °C and 35% RH are also included in Figure 18. As expected, the CGR for S31603 is much lower and is in the order of 1×10^{-12} m/s, which clearly shows the alloy effect.

From the results plotted in Figures 17 and 18, it can be concluded that the CGR from accelerated test at 50 °C is two orders of magnitude faster than the natural exposure condition at 27 °C. All the test data collectively indicate that CGR appears to be insensitive to the SIF, and CISCC can take place at a small threshold value (K_{ISCC}) even below 1 MPa√m. For the SRNL large plate test, Section 3.4.2 shows that the SIF calculated at the starter crack tips are in general higher than the load levels used in Kosaki tests (Figures 17 and 18). Therefore, it is expected that SCC in the SRNL large plate should have taken place. The reasons that no crack growth was observed on the plate surface could be that (i) the WRS may be altered or redistributed due to sectioning of the full size canister into the SRNL large plate and then by fabricating the EDM starter cracks; (ii) the crack growth is still under the incubation phase; and (iii) the naturally deliquescing salt

---

[3] The entire load range (K_I) in Kosaki accelerated tests for all specimen types is 0.3 to 32 MPa√m. Figure 21 only shows the data from semicircular specimens.

on the large plate surface did not reach the machined crack fronts, although water droplets at these locations refute this cause.

Crack initiation tests were also conducted by Kosaki [16]. Thin (1.5 mm in thickness) but non-cracked specimens were tested with four-point bend under the same natural exposure and accelerated test conditions [15, 16]. Only Type 304 test data from the natural exposure (average 27 °C and 80% RH) with 1.0 PS loading are used for discussion here, because the exposure condition is similar to the large plate test (nominally 22 °C and 73% RH) and the WRS could be at 1.0 PS level. The Kosaki data show that at least 993 and 364-573 days are required for a stress corrosion crack to initiate in the base metal and weld, respectively. Here the more conservative data obtained from the under glass method are referenced. Therefore, the Kosaki experiments seemed to imply that, even though the WRS is sufficient to cause stress corrosion crack growth, the incubation time could take as long as a year.

Note that the loadings used in Kosaki initiation tests with four-point bend specimens were 0.5 and 1.0 PS; and the loadings in his three-point bend CGR tests were 0.4 and 0.8 PS. Given the 0.2% yield stress of the mockup canister is 261 MPa (Table 2), the maximum welding residual stresses measured from the Sandia mockup canister (Figure 2) are summarized in Table 8. It can be seen that the WRS levels in the mockup canister are similar to the loading levels that were applied to the Kosaki specimens. Therefore, the Kosaki results on CGR and crack initiation [15, 16] may be relevant to the current large plate testing.

Table 8. Maximum welding residual stress measured from Sandia mockup canister

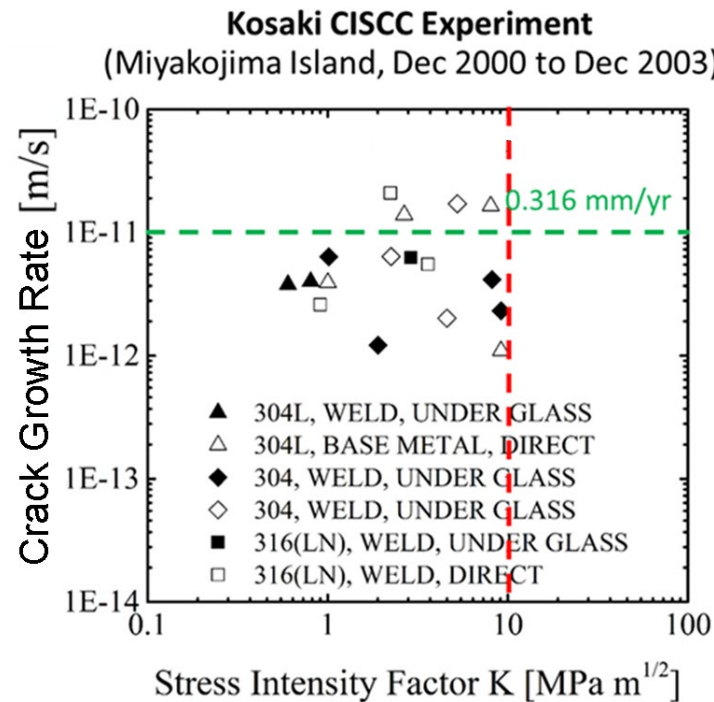| Location of WRS	WRS Component (see Figure 3)	Location of Max. Stress (see Figure 2)	Maximum Stress (1.0 PS = 261 MPa)
Weld Centerline	RS2 (WRS // Weld)	6 mm from OD	330 MPa (1.25 PS)
	RS3 (WRS ⊥ Weld)	7 mm from OD	110 MPa (0.42 PS)
Heat Affected Zone	RS2 (WRS // Weld)	1 mm from OD	210 MPa (0.80 PS)
	RS3 (WRS ⊥ Weld)	1 mm from OD	110 MPa (0.42 PS)

Figure 17. Crack growth rates from natural exposure on Miyakojima [15, 16] (Courtesy of Korea University under I-NERI/USA-ROK)
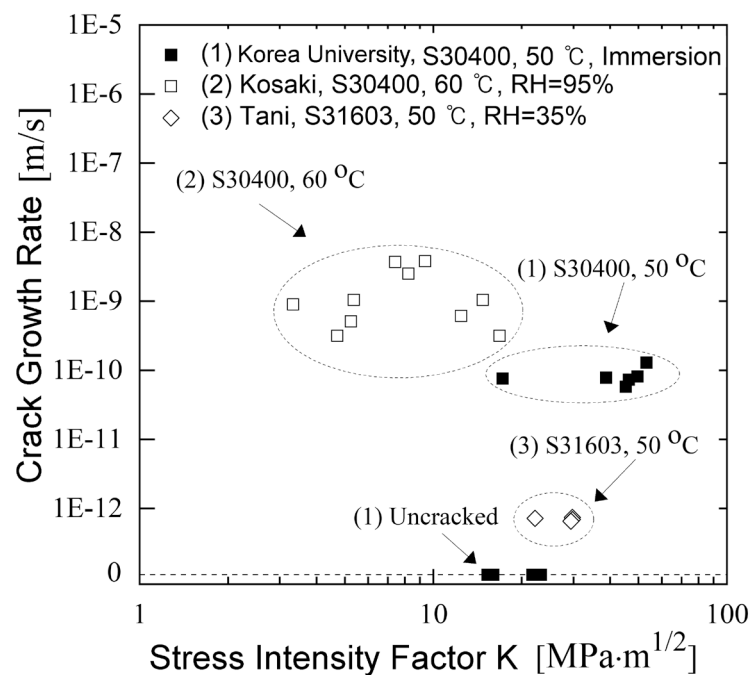

Figure 18. Crack growth rates from laboratory tests for stainless steels at 50 and 60°C under various CISCC conditions [19]

2.6.   Nondestructive Examination

The large plate was cleaned and inspected using visual inspection, liquid dye penetrant testing (PT), and ultrasonic testing (UT) inspected with dye penetrant tested to see if any evidence of SCC was visible on the outside surface of plate. No cracks were detected with this method.

Next, ultrasonic shearwave examination of the volume around the starter cracks was conducted. Figure 19 is a depiction of the scan plan as well as the indication in the second leg of the ultrasonic shearwave beam. The larger beam is a collective reflection of the beam spread at the bottom (corner trap) of the notch. The signal within the 1st leg being the diffracted tip from the top of the notch. The indication found in the EDM notch did not exceed the distance amplitude curve. Numerous factors can account for this either due to proximity of the indication to the corner trap, directional variations, or size. This indication however was declared by the UT inspector due to responses (reflections) from varying scanning positions which corelated to relatively the same depth. Measurements of the remaining ligament of the plate under VP-2 were 0.398 inches prior to the experiment and, 0.362 inches after. However, no crack extension was observed in the destructive examination at the notch tip.
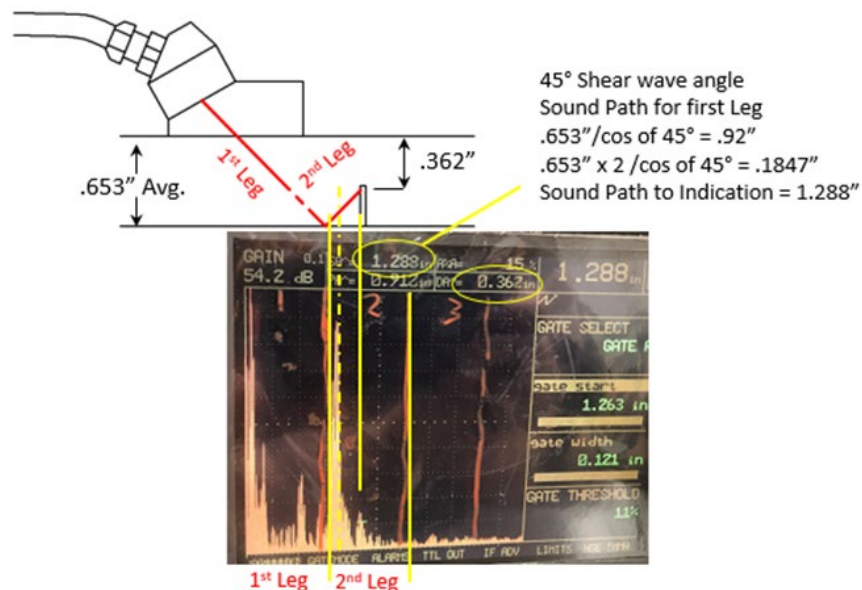
Figure 19. Ultrasonic Shearwave Examination of SRNL Large Plate Seed Crack VP-2 EDM Notch to detect stress corrosion cracking

2.7.   Destructive Examination

After the NDE results were observed, the decision was made to section the plate around VP-2 to confirm the results from the NDE examination. Samples were sectioned out of the large plate for a metallographic examination to reveal possible subsurface cracking and crack morphology. The

schematic is shown in Figure 20 and illustrates the method by which the sections were harvested from the plate. First, a circular section through the plate was cut using an EDM around the starter crack VP-2 (in center of cylinder). Then serial sectioning was performed using an EDM to create thin slices at regular intervals along the depth of the flaw. Table 9 contains the position of each sample relative to the top surface of the plate. The sample (slice) was mounted in metallographic mounting epoxy, ground and polished for imaging of the bottom surface of the sample. The specimens were not etched to avoid interfering with crack appearance.

Figures 21 - 31 contain images of crack like indications and pits on the inside surface of starter crack VP-2 at a depth of 0.06" below the outside surface of the plate. Areas labelled 1-28 span counter-clockwise (from top view) around perimeter of the starter crack as shown on image in Figure 20. Crack lengths ranging from 5 to 44 µm and pits up to 300 µm were observed.
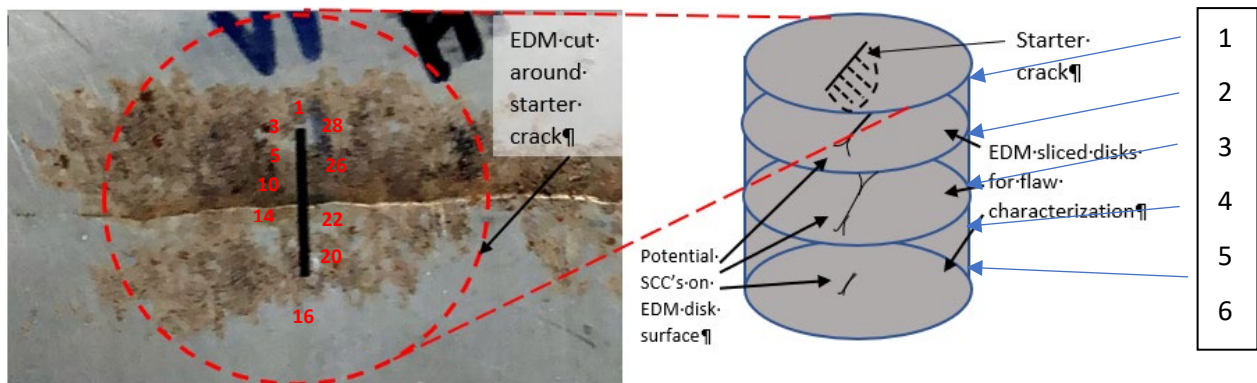
Figure 20. Schematic of serial sectioning of materials containing a starter crack VP-2 along the depth of the stress corrosion crack. Images from areas 1-13 and 24-28 are in the base metal. The other areas (14-23) are in the weld metal

Table 9: The position (depth) of each sample relative to the outside surface of the canister plate for starter crack VP-2

Sample #	Top Depth (inches)	Bottom Depth (inches)	Thickness (inches)	EDM length at top/bottom of sample disk (inches)
1	0	0.06	0.06	0.472/0.4569
2	0.075	0.127	0.052	0.4480/0.3983
3	0.142	0.195	0.053	0.3775/0.2666
4	0.210	0.266	0.056	0.2162/0.0
5	0.281	0.338	0.057	
6	0.353	0.418	0.065	
remainder	0.433	0.683	0.25	

TM-1000_0029   2021/08/03   18:36   100 um
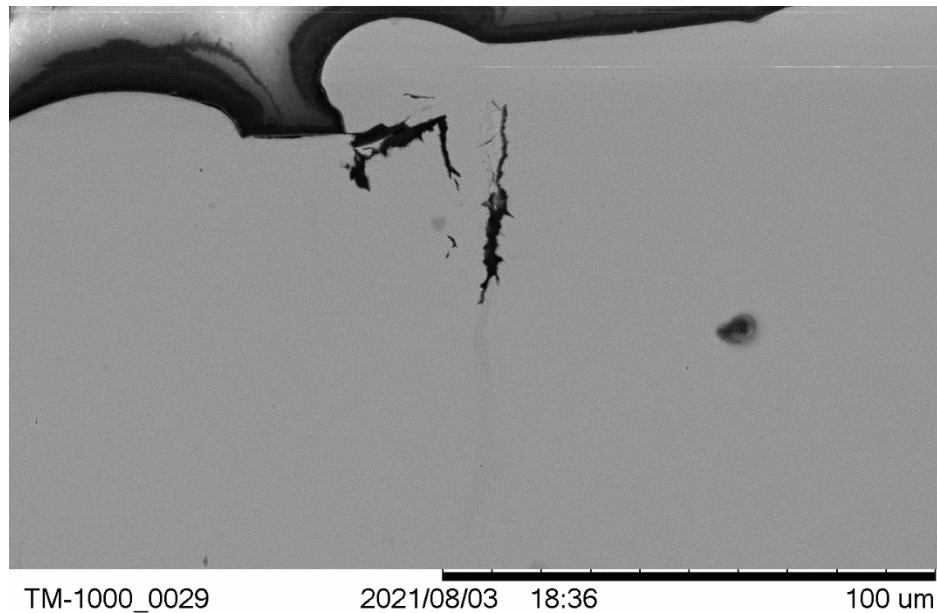
Figure 21 Secondary Electron Micrograph of Crack observed in Sample 1, Area 1. This image shows the 44 μm long stress corrosion crack, the maximum observed (base metal)

TM-1000_0035   2021/08/03   18:52   100 um

Figure 22 Secondary Electron Micrograph of Cracks observed in Sample 1, Area 3

Figure 23: Secondary Electron Micrograph of Cracks observed in Sample 1, Area 10
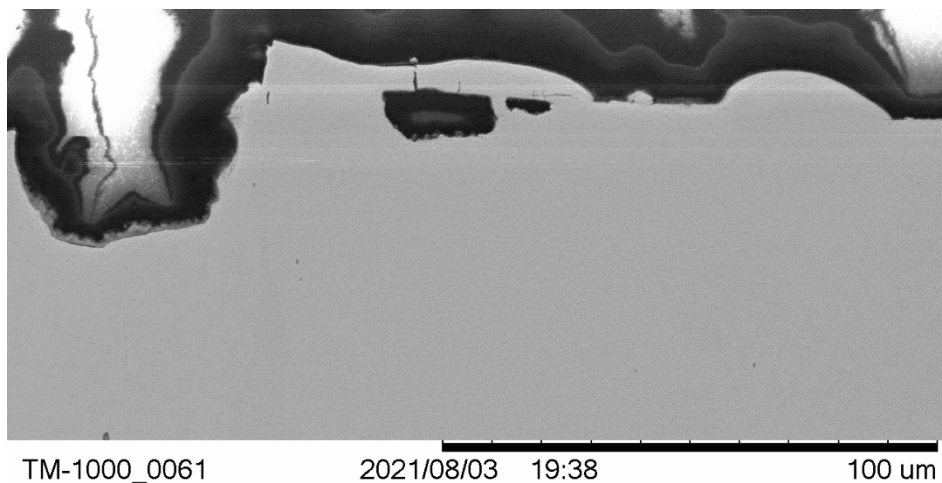
Figure 24: Secondary Electron Micrograph of Pits and Cracks observed in Sample 1, Area 5. Note that the Secondary Electron Micrograph images show artifact image features away from the sample surface that appear as cracks. These are not artifacts are not stress corrosion cracks in the stainless steel
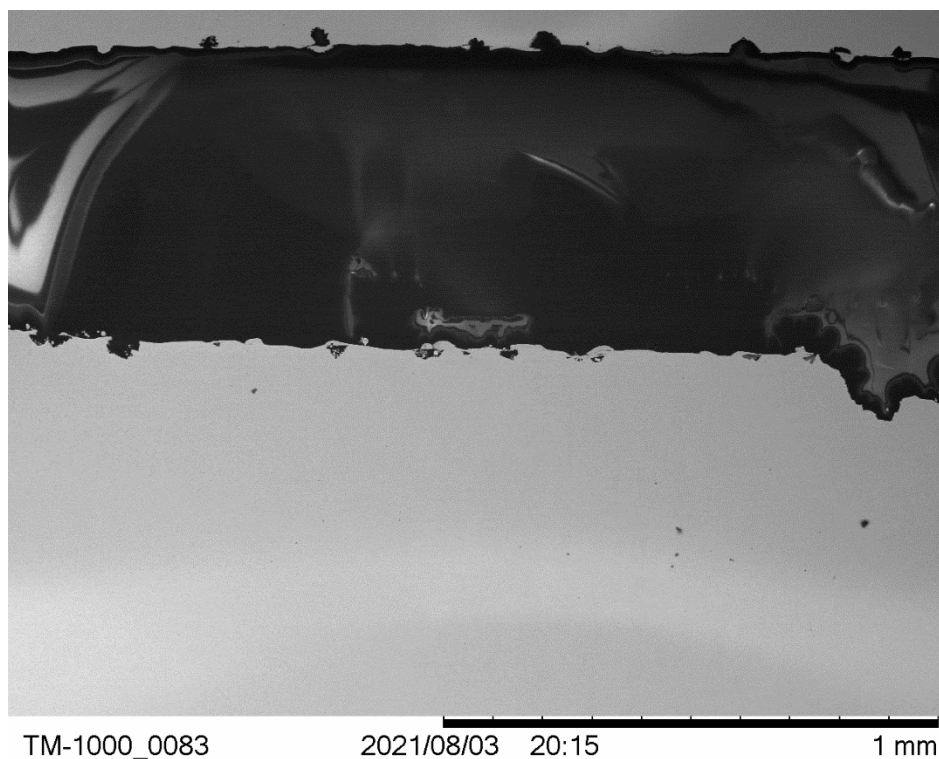
Figure 25: Secondary Electron Micrograph of Pits observed in Sample 1, Area 14
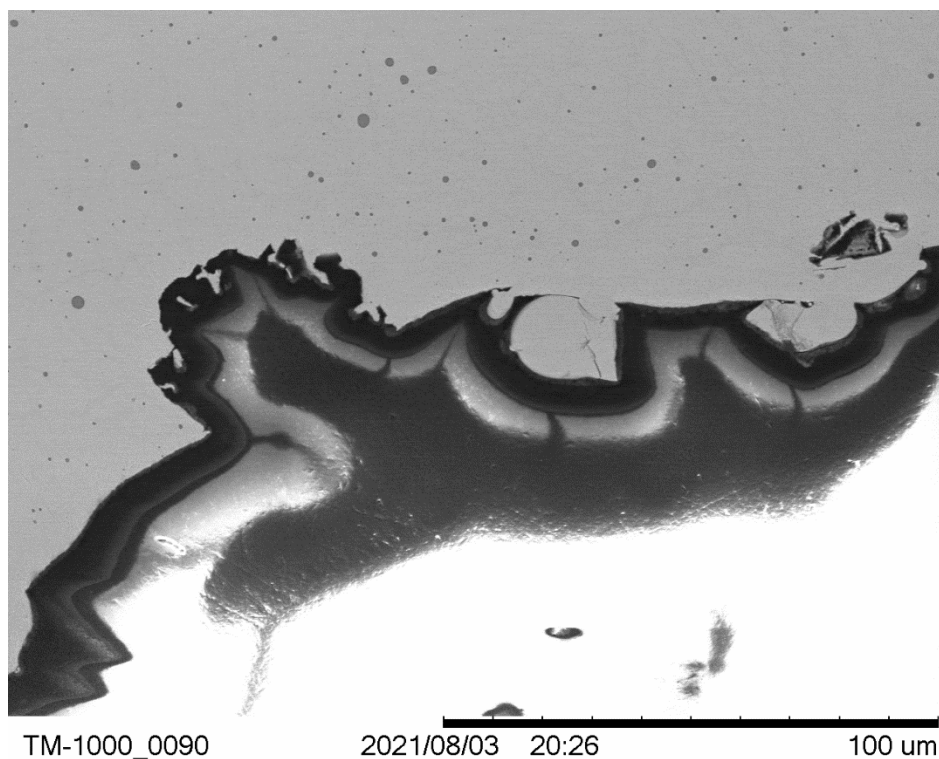
Figure 26: Secondary Electron Micrograph of Pits observed in Sample 1, Area 16
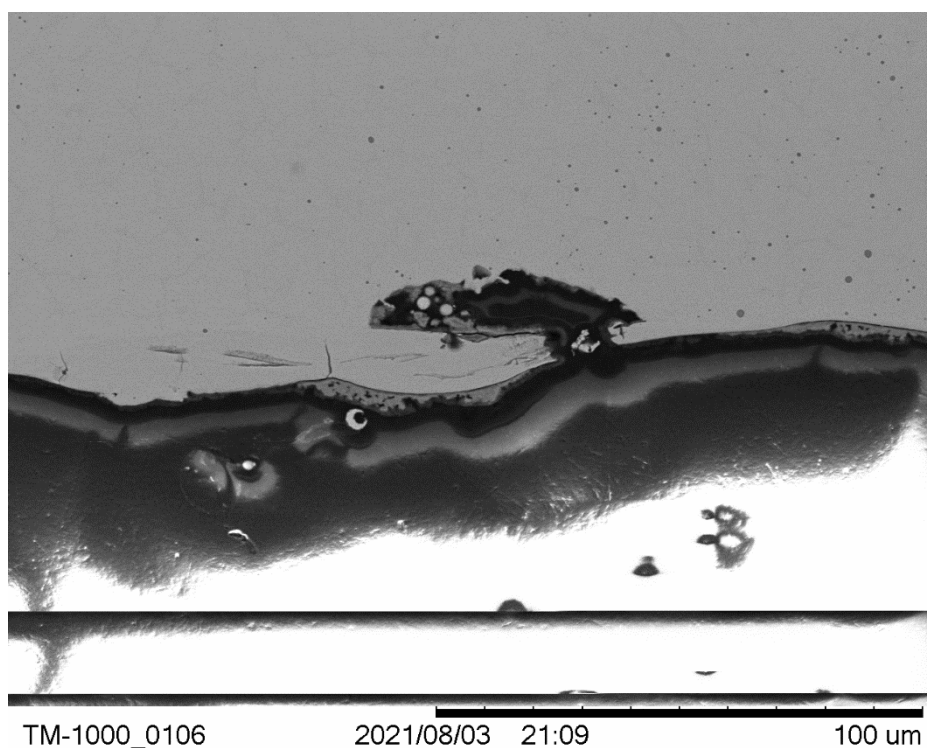
Figure 27: Secondary Electron Micrograph of Pits observed in Sample 1, Area 20

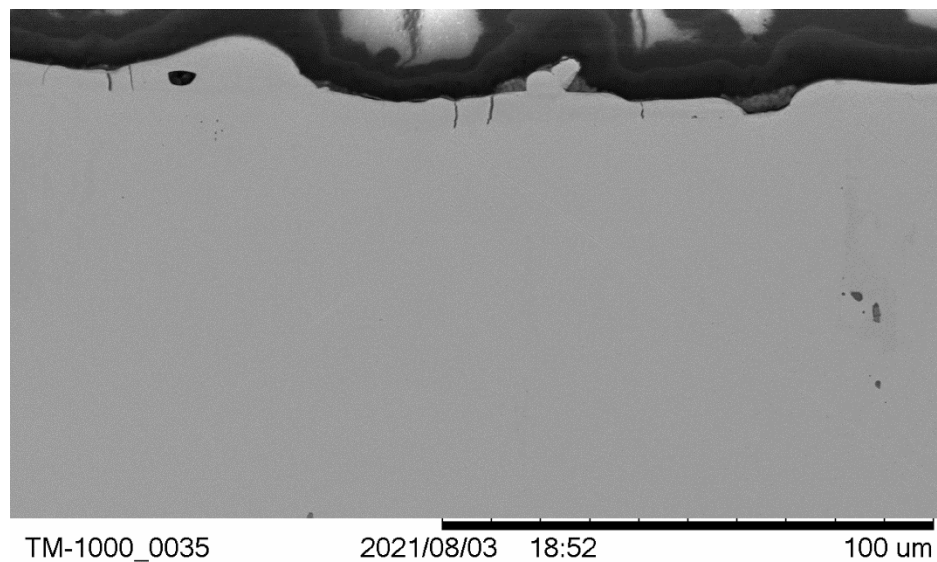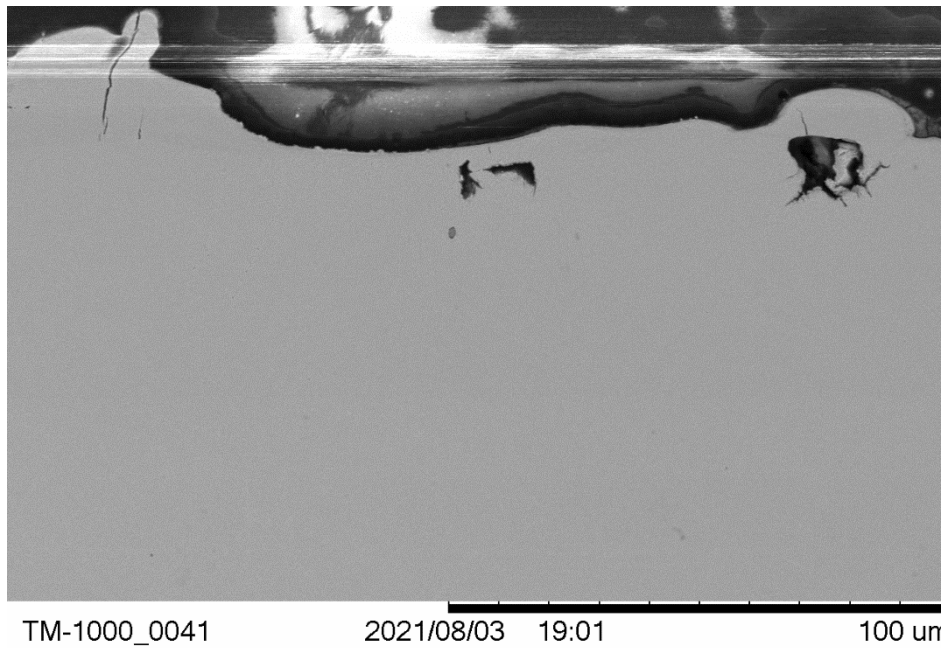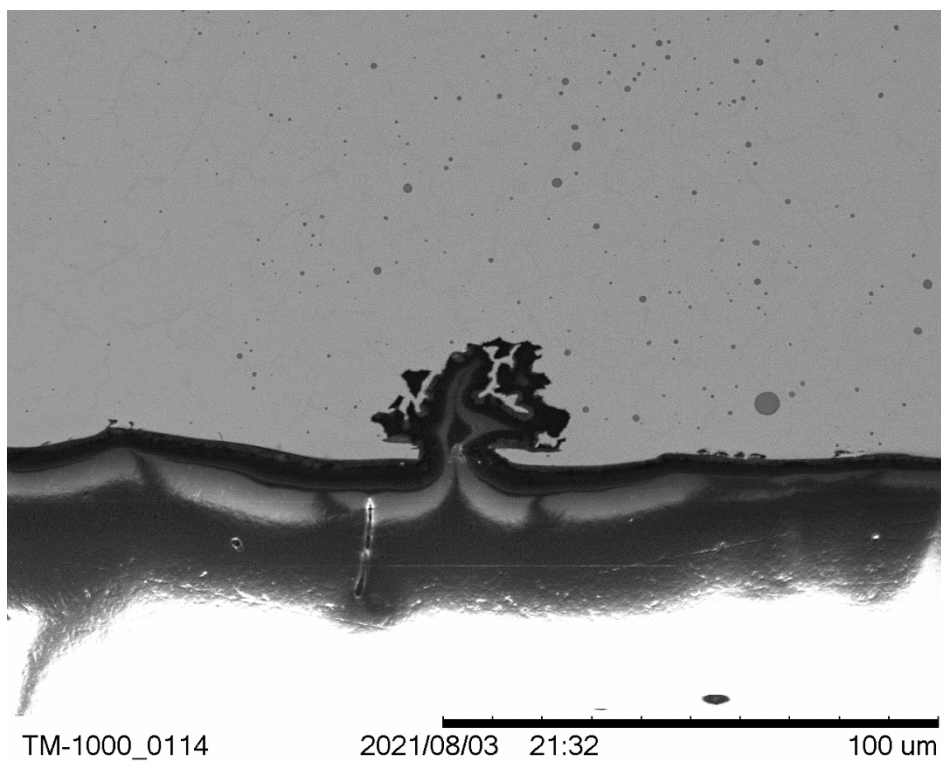**Figure 28: Secondary Electron Micrograph of Pits observed in Sample 1, Area 22**
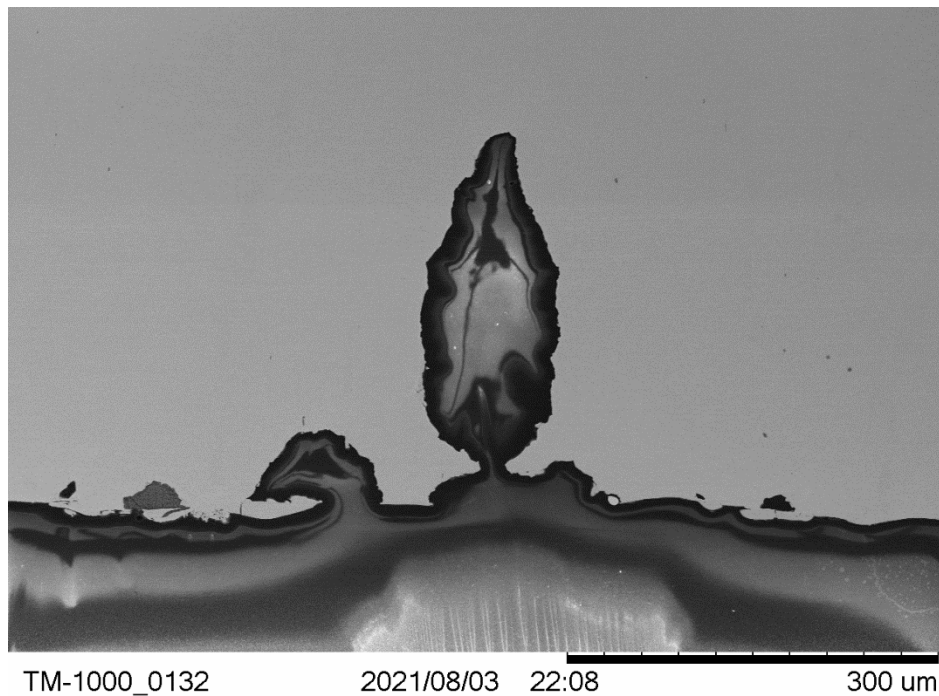
Figure 29: Secondary Electron Micrograph of Pits observed in Sample 1, Area 26 This image shows the 300 μm deep pit, the maximum observed (base metal)
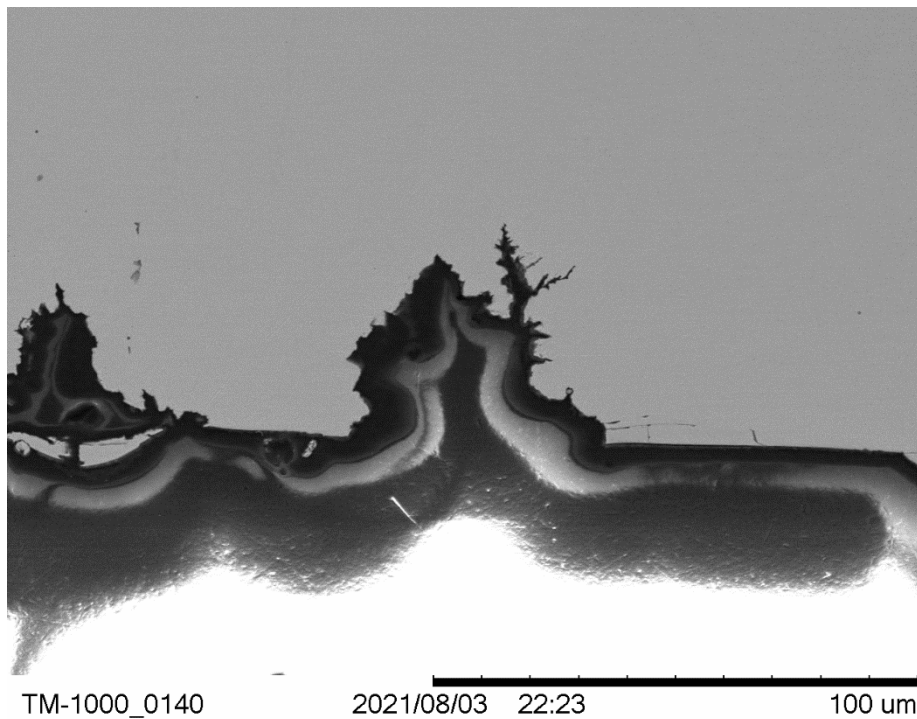
Figure 30: Secondary Electron Micrograph of Pits observed in Sample 1, Area 28
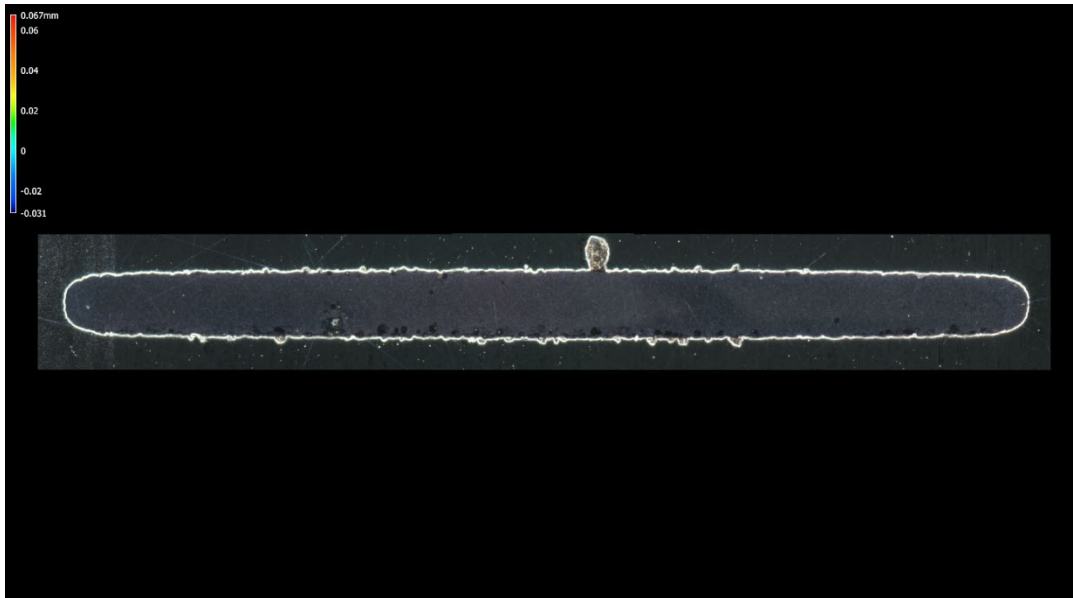
Figure 31: Optical Micrograph (using LCM) of Starter Crack, Sample 2. Chloride-induced pitting around the starter crack, in both base and weld metal is observed

3. ASME SECTION XI CODE CASE N-860 DEGRADATION ASSESSMENT

The SNL model [21] is shown below. The adjusted Crack growth rates for 295 K range between 36 µm/year and 5.3 mm/year. This model is similar to that used in the ASME code case [22] for canister in-service inspection.
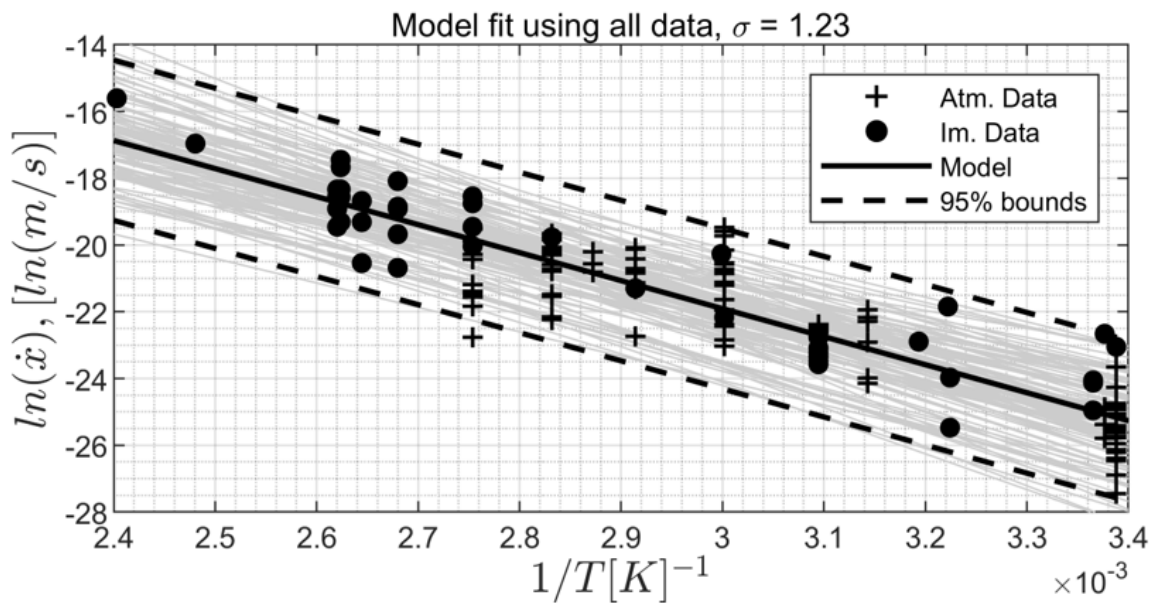
Figure 32: Crack Growth Rate as a function of Temperature [21]

The ASME Section XI Code Case N-860 [22] is intended to provide in-service inspection requirements for examination of the accessible exterior metallic portions of the welded austenitic stainless steel SNF storage and transportation canisters. In Code Case N-860 Paragraph 2320 "Classification of Degradation," the visual anomaly shall be classified by degradation condition and location. The Japanese Industrial Standard, JIS G 0595, "Rating Method of Rust and Stain of Atmospheric Corrosion for Stainless Steels," [23] is used as an example to distinguish the severity between "major," "minor," or "insignificant" degradation. The JIS G 0595 uses Rating Numbers (RN) to quantify the rust coverage on a 100×150 mm sample, with RN 0 representing 100% coverage and RN 9 being 0.0093%. The Code Case N-860 recommended that RN 0 to 4 indicates "major" surface corrosion (rust coverage > 22% on a 100×150 mm sample); RN 5 to 6 indicates "minor" surface corrosion (3% < rust coverage < 15%); and RN 7 and greater indicates "insignificant" surface corrosion (rust coverage < 0.4%).

This section describes degradation assessment to characterize large plate using JIS G 0595 method as suggested in ASME Section XI Code Case N-860. The weld area of the large plate is shown in Figure 25, which was taken on October 16, 2019. It was found that no significant changes of corrosion appearance since then, even after extra salt load was applied to two of the starter cracks (Fig. 12). As shown in Figure 25, a strict application of JIS G 0595 with a sampling size of 100×150 mm is not practical. Therefore, the rust coverage was performed over a 30×50 mm area (about 1/3 of the linear dimensions as required by JIS N 0595) around the seed crack VP2. Note that the design crack length of VP2 on the plate surface is 12 mm.

Figure 33. Rust coverage assessment for SRNL large plate: The yellow boxes represent JIS G 0595 region (100X150 mm), and a modified region (30X50 mm) currently used to evaluate starter crack VP2 and its vicinity, respectively

The estimation for the rust coverage can be described in three steps: (1) Image processing was performed over the 30×50 mm sampling region around starter crack (Figure 26a); (2) Masking the un-c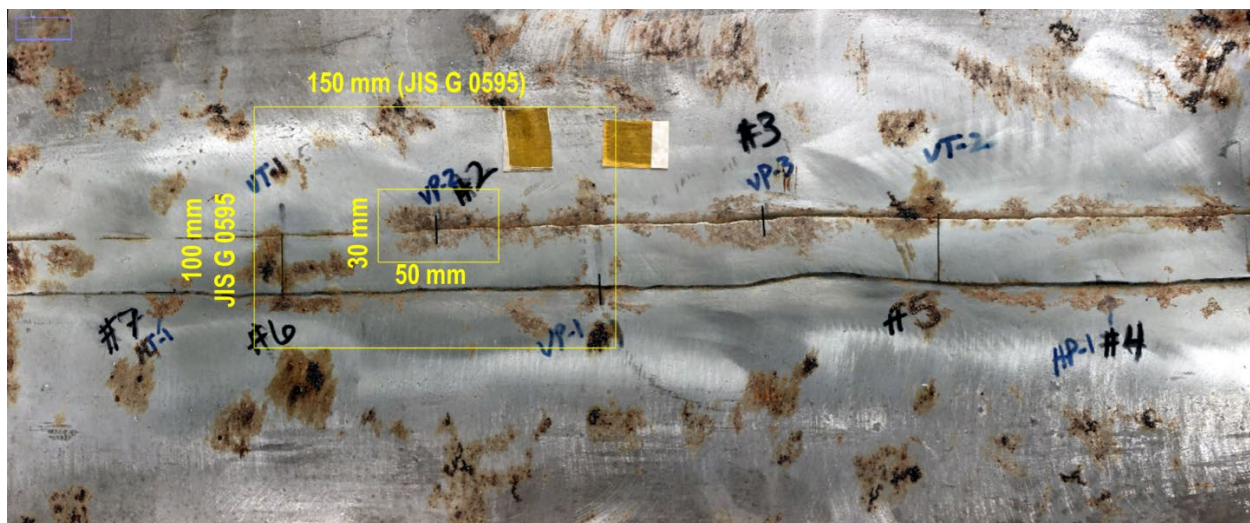orroded area in red over the sampling region (Figure 26b); and (3) Calculating the total pixel counts in the white area where the rust is identified (Figure 26c).

(a)   (b)   (c)
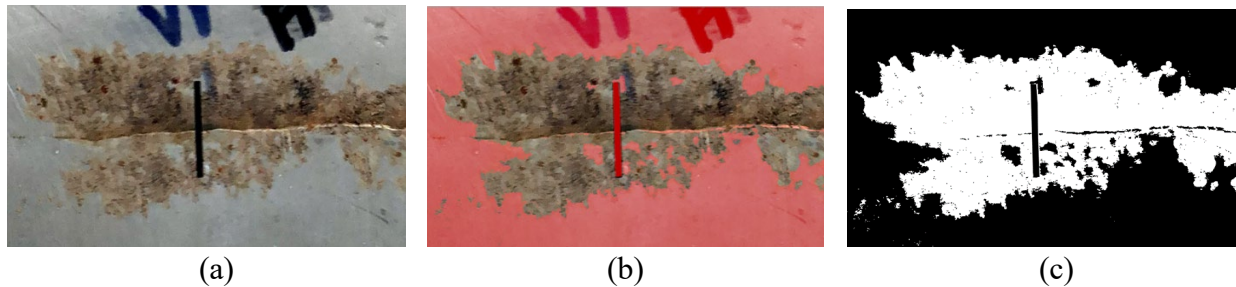
Figure 34. Image analysis to evaluate the rust coverage: sampled region (a), masking un-corroded area in red (b), and calculation of the white pixel counts in the rusted areas (c)

The pixel analysis result indicates that the corroded area in Figure 26c contains 170,403 pixels. With 420,336 total pixels in the entire sampling region (Figure 26a), the rust area ratio is 170,403/420,336= 40.5%. By JIS G 0595 designation, it is between RN 2 (47%) and RN 3 (32%).

By observing the Sandia big plate test images in Figures 21b and 22b, the corrosion condition appears more severe than the sampling region shown in Figure 26a. This is expected because Sandia big plates were heavily loaded with 8 g/m^2 of $MgCl_2$ and tested at 80 °C and 35% RH, and yet the SRNL large plate was loaded with less aggressive artificial sea salt with 2.3 grams Cl^-/m^2 and exposed to room temperature about 22 °C and 73% RH. If the same image process methodology would have been applied, the Sandia big plates would exceed RN 1 (69% rust coverage). Therefore, based on ASME Code Case N-860 recommendation, both Sandia and SRNL plates would be under the category of "major" surface corrosion (i.e., rust coverage > 22% on a 100×150 mm sample), and may require additional actions. On the other hand, if any corrosion is found in the weld region (Class C, as defined in Code Case N-860), then supplement examination such as surface or volumetric examination must be carried out, regardless of the surface corrosion classification (i.e., major, minor, or insignificant degradation). In the present case, both Sandia big plates and the SRNL large plate did not reveal any surface cracking for up through 2-years of exposure. It can be concluded that JIS G 0595 analysis is not sufficient to correlate CISCC to the surface corrosion condition.

4. CONCLUDING REMARKS

A large plate experiment in the laboratory was conducted to interrogate chloride-induced stress corrosion cracking (CISCC) crack growth behavior with a material and at an exposure condition pertinent to the extended storage of a spent nuclear fuel canister. The details of the experiment and the results are provided in this report.

The experimental design involving defects machined into the canister plate to provide sites for stress corrosion crack formation did result in causing SCC. All defects were characterized by NDE. Only defect VP-2 was destructively examined, and SCC was conclusively detected only by the DE. Using the assumption that there is no crack initiation period, several findings are made:

1. The SCC formation was not an extension from the initial EDM defect as hypothesized. There was no correlation of the crack size to the stress intensity factor calculated for the defect in the weld residual stress field. The SCC appeared to be approximately perpendicular to the EDM defect around its circumference
2. Only very small SCC was observed with a maximum crack growth of 44 µm or 22 µm/year crack growth rate. This crack growth rate is less than the lower 95% confidence bound of the literature data as compiled and modeled by SNL for the test temperature (22°C). This model is also used in the ASME N-860 code case
3. No particular correlation between pitting and SCC was observed. Pits, up to the maximum of 300 µm depth were observed

Etching and additional characterization of the VP-2 pits and cracks will be performed to compare to recent observations by SNL on pitting morphology, and to characterize the cracking as predominantly intergranular, transgranular, or mixed mode.

No additional CISCC experiments have been planned for the large plate remnant.   The plate remnant will be offered to Lucy Yu at UofSC for her NEUP investigation [24, 25].

5. REFERENCES

[1] Enos, D. G. and Bryan, C. R., 2016, *Final report: Characterization of Canister Mockup Weld Residual Stresses*, FCRD-UFD-2016-000064 Sandia National Laboratories, Albuquerque, New Mexico, USA.

[2] API 579-1/ASME FFS-1, 2007, Fitness-For-Service (API 579 Second Edition), American Petroleum Institute, Washington, DC., USA.

[3] API 579-1/ASME FFS-1, 2016, Fitness-For-Service, American Petroleum Institute, Washington, DC., USA.

[4] Lee, H. J., Kim, Y. J., Lam, P. S., and Sindelar, R. L., 2019, "Engineering J estimates for Spent Fuel Canisters under Combined Mechanical and Welding Residual Stresses,"

Paper Number PVP2019-93936, Proceedings of the ASME Pressure Vessels & Piping Conference, San Antonio, Texas, USA, July 2019.

[5]   Lam, P. S., Duncan, A. J., Ward, L. N., Sindelar, R. L., Kim, Y. J., Jeong, J. Y., Lee, H. J., and Lee, M. W., 2019, "Crack Growth Rate Testing and Large Plate Demonstration under Chloride-Induced Stress Corrosion Cracking Conditions in Stainless Steel Canisters for Storage of Spent Nuclear Fuel," Paper Number PVP2019-94031, Proceedings of the ASME Pressure Vessels & Piping Conference, San Antonio, Texas, USA.

[6] Duncan, A. J., Lam, P. S. and Sindelar, R. L., 2020, "CISCC Experiment of a Large Plate Sectioned from a Spent Nuclear Fuel Canister," Paper No. PVP2020-21774, Proceedings of the ASME Pressure Vessels & Piping Conference, Minneapolis, Minnesota, USA, July 2020.

[7]   Lam, P. S., Duncan, A. J., and Sindelar, R. L., Crack Growth Rate and Large Plate Demonstration of Chloride-induced Stress Corrosion Cracking in Spent Nuclear Fuel Storage Canisters, Milestone No. M3SF-19SR010201052 (SRNL-STI-2019-00561), September 2019, Savannah River National Laboratory, Aiken, South Carolina, USA.

[8]   Lam, P. S., Duncan, A. J., and Sindelar, R. L., Bryan, C. R., Large Plate Experiment of Chloride-induced Stress Corrosion Cracking in Spent Nuclear Fuel Storage Canisters, M3SF-20SR010207022 (SRNL-STI-2020-00315), September 2020, Savannah River National Laboratory, Aiken, South Carolina, USA.

[9]   Lam, P. S., Chang, C., Chao, Y. J., Sindelar, R. L., Stefek, T. M., and Elder III, J. B., 2005, "Stress Corrosion Cracking of Carbon Steel Weldments," Paper Number PVP2005-71327, Proceedings of ASME Pressure Vessels and Piping Conference, Denver, Colorado, USA.

[10] Lam, P. S., 2009, Investigation of the Potential for Caustic Stress Corrosion Cracking of A537 Carbon Steel Nuclear Waste Tanks, SRNS-STI-2009-00564 Rev.1, Savannah River Nuclear Solutions, Aiken, South Carolina, USA.

[11] Lam, P. S., Stripling, C. S., Fisher, D. L., and Elder III, J. B., 2010, "Potential for Stress Corrosion Cracking of A537 Carbon Steel Nuclear Waste Tanks Containing Highly Caustic Solutions," Paper No. PVP2010-25117, Proceedings of ASME Pressure Vessels and Piping Conference, Bellevue, Washington, USA.

[12] Lam, P. S. and Kim, Y. J., 2016, I-NERI Project Number 2016-001-K: *Flaw Stability and Stress Corrosion Cracking of Austenitic Stainless Steel Canisters for Long Term Storage and Transportation of LWR Used Fuel*, U. S. Department of Energy - Office of Nuclear Energy, Washington D. C., USA.

[13] Gim, J. M., Kim, J. S., Kim, Y. J., and Lam, P. S., 2018, "FE welding residual stress analysis and validation for spent nuclear fuel canisters," Paper Number PVP2018-84857, Proceedings ASME Pressure Vessels & Piping Conference, Prague, Czech Republic.

[14] Wang, J. A., Payzant, A., Bunn, J., and An, K., 2018, *Neutron Residual Stress mapping for Spent Nuclear Fuel Storage Canister Weldment*, ORNL/TM-2018/827, Oak Ridge, Tennessee, USA.

[15] Kosaki, A., 2006, "SCC Propagation Rate of Type 304, 304L Steels under Oceanic Air Environment," Paper No. ICONE14-89271, Vol. 1, Plant Operations, Maintenance and

Life Cycle; Component Reliability and Materials Issues; Codes, Standards, Licensing and Regulatory Issues; Fuel Cycle and High Level Waste Management, International Conference on Nuclear Engineering, July 17-20, Miami, Florida, USA, pp. 443-450.

[16] Kosaki, A., 2008, "Evaluation Method of Corrosion Lifetime of Conventional Stainless Steel Canister under Oceanic Air Environment," Nuclear Engineering and Design, 238, pp. 1233-1240.

[17] Relative Humidity in Miyakojima, Japan, http://www.miyakojima.climatemps.com/humidity.php

[18] Jeong, J. Y., Lee, M. W., Kim, Y. J., Sindelar, R., and Duncan, A., 2019, "Development of an apparatus for chloride induced stress corrosion cracking test using immersion method with constant displacement condition," Paper No. PVP2019-93922, Proceedings of ASME Pressure Vessels and Piping Conference, San Antonio, Texas, USA.

[19] Jeong, J. Y., Lee, M. W., Kim, Y. J., Lam, P. S., and Duncan, A. J., 2020, "Chloride-Induced Stress Corrosion Cracking Tester for Austenitic Stainless Steel," Journal of Testing and Evaluation, 49, Published ahead of print, 03 August 2020, ASTM International, West Conshohocken, Pennsylvania, USA. (https://doi.org/10.1520/JTE20200115)

[20] Tani, J., Mayuzumi, M., Arai, T., and Hara, N., 2007, "Stress Corrosion Cracking Growth Rates of Candidate Canister Materials for Spent Nuclear Fuel Storage in Chloride-Containing Atmosphere," Materials Transactions, Vol. 48, No. 6, pp. 1431 to 1437.

[21] Porter, N. W., Brooks, D., Bryan, C., Katona, R. and Schaller, R., FY21 Status Report: Probabilistic SCC Model for SNF Dry Storage Canisters, M3SF-21SN010207057 (SAND2021-9213 R), July, 2021, Sandia National Laboratories, Albuquerque, New Mexico, USA.

[22] ASME Boiler and Pressure Vessel Section XI Code Case N-860: "Inspection Requirements and Evaluation Standards for Spent Nuclear Fuel Storage and Transportation Containment Systems," Board approved July 2020, in preparation for publication, American Society of Mechanical Engineers, New York, NY, USA.

[23] Japanese Industrial Standard, "Rating Method of Rust and Stain of Atmospheric Corrosion for Stainless Steels," JIS G 0595: 2004, Translated to English by Japanese Standards Association, January 2005.

[27] Yu, L., DOE Nuclear Energy University Program 2020, "Engineered composite patch with NDE inspection for repair and mitigation of SCC in nuclear spent fuel dry storage canister," University of South Carolina, Columbia, SC., USA.

[28] Yu, L., DOE Nuclear Energy University Program 2019, "Remote laser based nondestructive evaluation for post irradiation examination of accident tolerant fuel (ATF) cladding," University of South Carolina, Columbia, SC., USA.